International Journal of Earth Sciences (2021) 110:1477–1499
https://doi.org/10.1007/s00531-021-02025-9

ORIGINAL PAPER

The provenance signal of climate–tectonic interactions in the evolving St. Elias orogen: framework component analysis and pyroxene and epidote single grain geochemistry of sediments from IODP 341 sites U1417 and U1418

Barbara Huber[1] · **Heinrich Bahlburg**[1]

Received: 28 October 2020 / Accepted: 11 March 2021 / Published online: 2 April 2021

Abstract
The St. Elias orogen and the Surveyor Fan in the adjacent Gulf of Alaska are a coupled source to sink system recording the interplay of tectonics and variable degrees of glaciation during the collision of the Yakutat terrane with the southern Alaska margin since the Miocene. The Miocene to Holocene sediments of the Surveyor Fan were drilled during IODP expedition 341. The recovered material is used to constrain information on changes in erosion centers during the last 10 Ma to study the impact of climatic and tectonic processes on orogen evolution. Point counting of sand- and silt-sized light framework components and geochemical single grain analysis of heavy mineral groups epidote and pyroxene is applied to analyze patterns of sedimentary provenance of two sites on the distal and proximal Surveyor Fan (Site U1417 and U1418, respectively). The studied sands and silts of Miocene to Pleistocene age are slightly enriched in feldspar (plag >> kf) at the proximal site, compositions at both sites do not show systematical changes with time of deposition. Framework component spectra uniformly reflect the expected active margin provenance. Epidote and pyroxene compositions are very consistent and show no change with time of deposition. Associations of epidote and pyroxene with albite, titanite and pumpellyite are in line with near-shore sources in the Chugach Metamorphic Complex and the metabasite belt at its southern border, and in units of recycled detritus exposed in the fold and thrust belt on the western Yakutat Terrane, respectively. Rock fragments indicate input from mainly metamorphic sources during the Miocene and Pliocene and an increase of input from low-grade metamorphic and sedimentary rocks in the Pleistocene, a finding also indicated by the abundance of epidote and pyroxene. This implies increasing erosion of the near-shore areas of the fold and thrust belt with advance of glaciers to the shore since the Miocene, being enhanced by the onset of the Northern Hemisphere glaciation at the beginning of the Pleistocene. Climate changes connected to the mid-Pleistocene transition did not result in appreciable changes in the petrographic compositions. Glaciers seem to have remained nested in their topographically predefined positions, continuously feeding material with uniform characteristics into the fan.

Keywords Alaska · Provenance · Framework components · Pyroxene · Epidote · Climate–tectonic interactions

Introduction

The detritus constituting clastic sedimentary rocks is commonly derived from a multitude of source rocks and from several source regions (e.g. Garzanti and Andò 2007). It is therefore often difficult to determine specific provenance from such mixtures, in particular from old mountain belts of fragmentary preservation. Mountain belts may develop pronounced climatic asymmetries if they are oriented perpendicular to prevailing wind systems (Willett et al. 1993; Hay 1996). This results in significant material export being limited to the windward side of the evolving orogen. Sediment transfer paths are relatively short, if the windward side of accretionary, or exterior, coastal mountain belts (Cawood and Buchan 2007; Collins et al. 2011) is facing an ocean basin (Thornburg and Kulm 1987; Potter 1994; Koons et al. 2003; Roe et al. 2006). The stratigraphy and

✉ Heinrich Bahlburg
hbahlburg@wwu.de

[1] Institut für Geologie und Paläontologie, Westfälische Wilhelms-Universität, Münster, Germany

provenance of the detritus transported out of coastal accretionary mountain belts and into an adjacent ocean basin is thus much more likely to reflect the climatically and tectonically controlled exhumation history of the orogen without interference from external sources. The long-term sink for this sediment is often found in large submarine fans or trench systems where sediments accumulate at high rates of 35–120 cm/kyr relative to deep-sea pelagic sedimentation (Thornburg et al. 1990; Clift and Vannucchi 2004; Gulick et al. 2015; Bergmann et al. 2020; Garzanti et al. 2020; Pickering et al. 2020a; Reilly et al. 2020).

Mass export from a coastal mountain belt is enhanced if the orogen is affected by varying degrees of glaciation (Hallet et al. 1996; Berger et al. 2008; Koppes and Montgomery 2009; Gulick et al. 2015; Carter et al. 2017). The erosion of mountain ranges by glaciers varies with changes in average temperature resulting in potentially lower rates effected by cold-based glaciers during glacial intervals, and increased rates connected to Alpine glaciers during interglacial periods. These variations also depend on elevation and latitudinal position (Yanites & Ehlers 2012). Examples include the southern Andes and the adjacent overfilled trench (Thornburg et al. 1990; Contreras-Reyes et al. 2010), the Southern Alps and adjacent basins of New Zealand (Griffiths 1979; Jiao et al. 2018,), the Himalaya-Bengal Fan system (Bergmann et al. 2020; Pickering et al. 2020b; Reilly et al. 2020), and the St. Elias orogen in southern Alaska and the adjacent Surveyor Fan (Plafker et al. 1994; Reece et al. 2011; Gulick et al. 2015; Huber et al. 2018a,b; Bootes et al. 2019).

The present provenance study enlarges upon the data presented by Huber et al. (2018a,b) which considered U–Pb detrital zircon age and Hf isotope data together with geochemical heavy mineral data on garnet and amphibole recovered by IODP Expedition 341 at sites U1417 and U1418 on the distal and proximal Surveyor Fan, respectively (Fig. 1a). Here, we augment this information by examining the framework component distribution of selected sand and silt layers together with the single grain geochemistry of detrital pyroxene and epidote.

We will use our new data to assess changes in the detrital component compositions of the Gulf of Alaska sediment since the middle Miocene. This will be conducive to further constraining consistencies or variabilities in the source to sink relationship between the main erosion centers in the evolving St. Elias orogen and the Surveyor Fan transport and depositional system. Linking the stratigraphic age and composition of the Gulf of Alaska sediments to the mainland glacial and tectonic history will help to understand the selective impact of glacial and tectonic processes on the rates and foci of exhumation and erosion.

The example of the St. Elias orogen-Surveyor Fan source to sink system

The southern Alaska continental margin hosts the highest coastal mountain range on Earth, the St. Elias Mountains. It formed in the last ca. 8 Ma through accretion and subduction of the Yakutat terrane, and at a time of glaciation of variable intensity (Plafker et al. 1994; Bruhn et al. 2004; Enkelmann et al. 2008, 2015; Finzel et al. 2011, 2015; Pavlis et al. 2012; Falkowski et al. 2014). The windward side of the orogen faces the Gulf of Alaska. The interplay of climate and tectonics during orogeny since the Miocene shaped its exhumation and erosion history the information on which is stored in the Gulf of Alaska sediment, and mainly in the Surveyor Fan (Plafker et al. 1994; Gulick et al. 2015). This was originally shown by DSDP Leg 18 (Kulm et al. 1973) and was enlarged upon by IODP Expedition 341 (Expedition 341 Scientists 2014; Jaeger et al. 2014). The St. Elias orogen-Surveyor Fan source to sink system is one of the key natural laboratories to study climate–tectonic interactions during mountain building (Gulick et al. 2015).

Provenance framework of the St. Elias orogen

A variety of provenance and thermochronological data derived from the rocks constituting the St. Elias orogen and the sediments of the Gulf of Alaska allowed for tracing the spatial and temporal development of erosion of and mass transfer from the orogen. These data constrain the main source areas to the Chugach Terrane (Huber et al. 2018a,b), a mainly metasedimentary accretionary complex of upper Cretaceous age (Fig. 1; Pavlis and Sisson 1995; Barefoot et al. 2020). The St. Elias syntax at the transition from the strike-slip Fairweather Fault to the Chugach-St. Elias thrust fault registers the highest rates of erosion, exhumation and uplift (Fig. 1; Falkowski et al. 2014; Dunn et al. 2017; Enkelmann et al. 2017; Huber et al. 2018a,b; Bootes et al. 2019). The Fairweather Fault, in turn, is the fastest-slipping intracontinental strike-slip fault on decadal to millennial time scales (Molnar and Dayem 2010; Lease et al. 2021).

Tectonic setting

The St. Elias orogen at the southern Alaska continental margin formed through the successive accretion of several allochthonous terranes against the North American continent (Coney et al. 1980; Plafker et al. 1994; Colpron et al. 2007). South of the Border Ranges Fault (Fig. 1a, b), accreted terranes, namely the Yakutat, Prince William and Chugach terranes form a broad accretionary complex accreted against

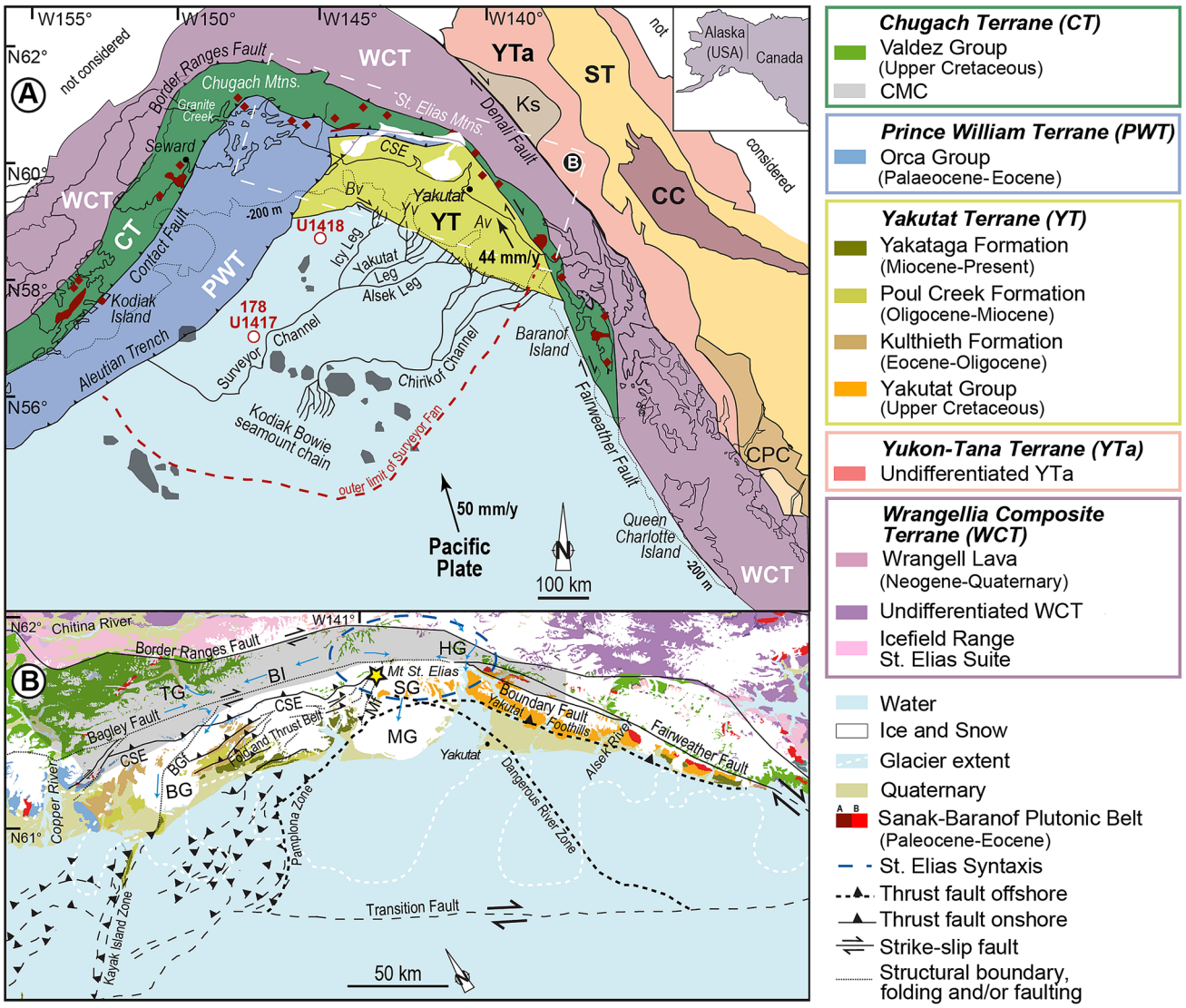

Fig. 1 **a** Terrane map of the southern Alaska continental margin (modified after Huber et al. (2018b) and references therein. CC = Cache Creek Terrane, CT = Chugach Terrane, PWT = Prince William Terrane, ST = Stikinia Terrane, WCT = Wrangellia composite Terrane, YT = Yakutat Terrane, YTa = Yukon-Tana Terrane; Av = Alsek valley, Bv = Bering valley, CPC = Coast Plutonic Complex, CSE = Chugach-St. Elias Fault, KS = Kluane Schist, Yv = Yakutat valley. Red circles mark the distal (U1417) and proximal (U1418) sites of IODP Expedition 341, and Site 178 of DSDP Leg 18. **b** Simplified geological map of the southern Alaska continental margin. BG = Bering Glacier, BGf = Bering Glacier Fault, BI = Bagley Icefield, CSE = Chugach-St. Elias Fault, HG = Hubbard Glacier, Mf = Malaspina Fault, MG = Malaspina Glacier, SG = Seward Glacier, TG = Tana Glacier. Blue arrows indicate glacial flow directions according to Post (1972). The glacier extent during the Last Glacial Maximum after Manley and Kaufman (2002) is marked with a white dashed line. The extent of the Chugach metamorphic complex (CMC) is marked by the gray shaded area. Plate velocity vectors are from Pavlis et al. (2012)

the Wrangellia composite terrane (Fig. 1b). Wrangellia had been accreted already in Middle Jurassic to Late Cretaceous time (Trop et al. 2002). The St. Elias orogen developed due to ongoing NW directed subduction of the Yakutat terrane presently taking place at a rate of 50 mm year^{-1} relative to the North American plate (Fig. 1a; Elliott et al. 2010; Gulick et al. 2015). In the course of these developments, western Alaska also experienced counterclockwise rotation (Plafker 1987).

The Chugach and Prince William terranes consist mainly of coherent or disrupted turbidite successions and associated melange zones included in the Valdez and Orca groups of Upper Cretaceous-Eocene age (Fig. 1). The deposits originally represent forearc and trench deposits linked to a submarine fan system accumulated by sedimentation rates higher than those of the Bengal-Nicobar fan system (Nilsen and Zuffa 1982; Sample and Reid 2003). The rocks are preserved in greenschist to sub-greenschist metamorphic grade.

Along the present suture to the Yakutat terrane, this complex is more strongly deformed and the metamorphism reaches upper amphibolite metamorphic grade (Pavlis and Sisson 1995). Metamorphism is connected to Eocene ridge subduction and the intrusion of the approximately 2100 km long forearc intrusive zone of the Sanak-Baranof Plutonic Belt (SBPB) between ca. 60 and 50 Ma (Sisson et al. 1989, 2003; Bradley et al. 1993, 2003; Plafker et al. 1994; Pavlis and Sisson 1995; Haeussler et al. 2003; Farris and Paterson 2009). This higher-grade equivalent of the Valdez and Orca groups is ca. 350 km long and is named the Chugach Metamorphic Complex (Hudson and Plafker 1982; Bruand et al. 2011; Gasser et al. 2011). A metabasite belt of amphibolite facies is juxtaposed against the Chugach Metamorphic Complex along the Contact and Fairweather faults, facing lower-grade metamorphic rocks to the south (Fig. 1; Bruand et al. 2011; Gasser et al. 2011).

The most outboard terrane, the Yakutat terrane, is tied to the movement of the Pacific plate and is the latest terrane accreting to the southern Alaska margin (Plafker et al. 1994). Northwestward transport of the Yakutat terrane along the dextral Fairweather transform fault system since ca. 30 Ma led to subduction of the Yakutat slab and accretion of the Yakutat terrane along the Chugach-St. Elias and Bering Glacier faults (CSE and BGf, respectively, in Fig. 1b). Since the Miocene, this drove the formation of the St. Elias Mountains (Plafker 1987; Plafker et al. 1994; Bruhn et al. 2004; Enkelmann et al. 2008, 2015; Finzel et al. 2011; Arkle et al. 2013; Falkowski et al. 2014). Strong uplift and erosion characterize the orogeny during the last ca. 10 Ma, especially at the Yakutat plate corner, also named the St. Elias Syntaxis, where the transform motion along the Fairweather Fault changes to flat-slab subduction along the Chugach-St. Elias Fault (Fig. 1; Pavlis et al. 2012; Enkelmann et al. 2009, 2010, 2015, 2017; Falkowski et al. 2014; Dunn et al. 2017).

The accreting Yakutat terrane is characterized by a fold and thrust belt located seaward of the Chugach-St. Elias Fault and particularly well developed in its western part (Fig. 1b; Plafker et al. 1994; Enkelmann et al., 2010). It consists of imbricated sediments scraped off the basement and organized into the pre-orogenic Kulthieth (Eocene–Oligocene), Poul Creek (Lower Oligocene to Lower Miocene) and the syn-orogenic Yakataga (Miocene through Holocene) formations (Plafker 1987; Plafker et al. 1994; Worthington et al. 2010; Enkelmann et al. 2015). The eastern part of the terrane is covered by the Upper Cretaceous Yakutat Group comprising fluvial and glaciomarine syn-orogenic strata. It is part of the Chugach flysch and mélange predating the fold and thrust belt development (Plafker 1987; Plafker et al. 1994; Pavlis et al. 2012).

The origin and transport history of the Yakutat Terrane are under debate. The far-travelled terrane hypothesis proposes an origin 1500–2000 km to the south at ca. 44° paleonorth or close to northern California and southern Oregon in the Eocene (Bruns 1983). The short transport hypothesis (ca. 600 km) appears to be more in line with available data and places the origin of the terrane near Prince Rupert, British Columbia (Plafker et al. 1994; Perry et al. 2009).

Changing degrees of glaciation

Alpine glaciation at the Southern Alaskan continental margin started in the late Miocene (ca. 7 Ma) shortly after the onset of the formation of the St. Elias orogen. It expanded to tidewater glaciation between 6.7 and 5.0 Ma (Lagoe et al. 1993; Fig. 2). After a warm mid-Pliocene period from 4.2 to ca. 3 Ma, the Northern Hemisphere glaciation intensified at ca. 2.7 Ma when global glacial–interglacial climate cycles changed from 40 to 100 kyr at 0.7 to 1 Ma during the mid-Pleistocene transition (Lagoe et al. 1993; Lagoe and Zellers 1996). Beginning at this time, glaciers extended onto the shelf. This coincided with inception of the Surveyor Channel feeding the Surveyor fan (Reece et al. 2011; Gulick et al. 2015). Dropstones recovered at Site U1417 record drifting icebergs by ca. 2.6 Ma (Jaeger et al. 2014; Gulick et al. 2015).

The depositional precursor systems of today's Surveyor fan have been active since ca. 9.7 Ma, moving to the northwest with the Pacific Plate since onset of deposition (Plafker 1987; Stevenson and Embley 1987; Rea and Snoeckx 1995; Reece et al. 2011). How sediment was transported into the precursor of today's Surveyor fan during the early stages of deposition is not resolved so far. The absence of a glacial transport system as well as implications from heavy mineral, zircon U–Pb age and seismic reflection data of the early fan sediments implies the presence of a fluvial tributary system before the onset of glaciation in the late Miocene, funneling material from sources in the North (Stevenson and Embley 1987; Huber et al. 2018a, b).

Today, the Bering, Malaspina and Hubbard glaciers are the largest glaciers of southern Alaska (Pewé 1975; BG, MG and HG in Fig. 1b). The glacial systems directly feed orogenic detritus into today's Surveyor Fan through the Surveyor Channel system which discharges into the Aleutian Trench at its distal end (Fig. 1). The outlets of the glacier systems towards the Gulf of Alaska appear to be tectonically and morphologically controlled as they coincide with major thrust systems. The Bering glacier follows the eastward extension of the Kayak Island Zone, the Malaspina Glacier connects to the continuation on land of the Pamplona Zone (Fig. 1b).

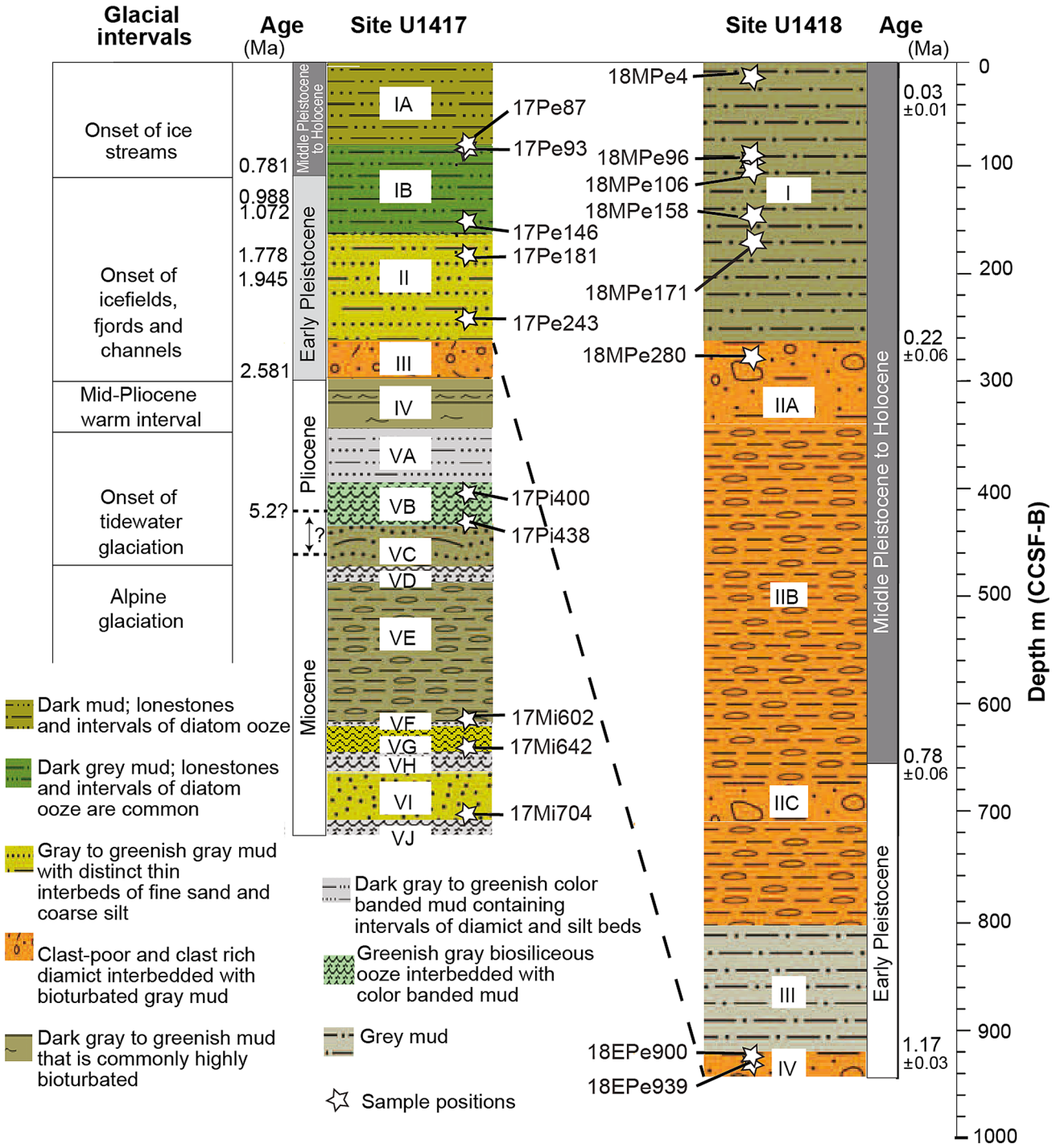

Fig. 2 Lithostratigraphy of IODP Expedition 341 sites U1417 (distal site) and U1418 (proximal site) and climatic events in Southern Alaska. Sample positions are marked with white stars. Modified after Lagoe et al. (1993) and Expedition 341 Scientists (2014)

Samples

Samples were taken from fine to medium sands and silts of IODP Expedition 341 sites U1417 and U1418. Site U1417 was drilled ca. 60 km west of today's Surveyor Channel in the distal Surveyor Fan, today being fed by the Alsek, Yakutat and Icy legs through hemipelagic/pelagic rainout and overbank levee deposition from turbidity currents (Expedition 341 Scientists 2014; Dunn et al. 2017; Fig. 1a). Sediments from a maximum depth of ca. 700 m below sea floor of Miocene (ca. 10 Ma) to Holocene age were recovered (Fig. 2). Site U1418 recovered ca. 950 m

of Early Pleistocene to Holocene sediments from the proximal Surveyor Fan (Expedition 341 Scientists 2014) (Fig. 2). The lowermost lithostratigraphic unit IV formed through an Early Pleistocene massive slope failure (mass transport deposit) (Reece et al. 2011; Expedition 341 Scientists 2014). All younger units were deposited through hemipelagic settling and by overbank turbidity currents from nearby channels (Reece et al. 2011; Expedition 341 Scientists 2014).

Sample names start with the abbreviated name of the site (17 for U1417 or 18 for U1418) followed by the abbreviated name of the stratigraphic interval (Mi = Miocene, Pi = Pliocene, Pe = Pleistocene, EPe = Early Pleistocene, MPe = Middle Pleistocene) and the sampling depth in m core composite depth below seafloor (m CCSF-B) (Fig. 2). The IODP code of each sample can be found in Appendix A. Deposition ages were deduced from bio- and magnetostratigraphic reconstructions and the resulting age model (Expedition 341 Scientists 2014; Jaeger et al. 2014; Gulick et al. 2015; Fig. 2). The sample volume is limited by the amount of material recovered in the sediment core half provided for sampling.

Grains < 0.063 mm provide the largest fraction in all samples, making up over 90% in some samples. Grains > 0.25 mm make up only 0–2% in most samples. The heavy mineral content in all samples is moderately rich (< 5%). The absolute heavy mineral volume for analysis is small. Sediment volumes are limited because of the diameter of the drill core (6.2 cm; sample weights of ca. 10 g to 70 g) and grain size, with many samples providing < 1.5 g of material of 0.063–0.25 mm. Still, this size fraction was the only one providing valuable amounts of heavy minerals for analysis. The small sample volume also made the calculation of sample indices like the Heavy Mineral Concentration index (Garzanti et al. 2007) unfeasible. Restriction to this narrow grain size fraction might lead to some information being lost because of grain size dependence of mineral compositions (e.g., Garzanti et al. 2008; Krippner et al. 2014). Still, intersample comparison is not invalidated (Huber et al. 2018b).

Methods

The provenance tool box

Provenance research is most effective when several provenance tools are combined (von Eynatten et al. 2003; Weltje and von Eynatten 2004; von Eynatten and Dunkl 2012; Reimann et al. 2015; Garzanti 2016). This allows the derivation of information on a wide range of source lithologies and their specific origins to approach a comprehensive reconstruction of provenance.

Amphibole and garnet are widely used provenance tracers (Mange and Morton 2007; Andò et al. 2014; Krippner et al. 2014; Caracciolo et al. 2016; Hülscher et al. 2018; Huber et al. 2018b; Liang et al. 2019). Pyroxene geochemistry reveals information mainly on mafic source rock types and their plate tectonic setting (Nisbet and Pearce 1977; Cawood 1983; Morimoto et al. 1988; Nechaev and Isphording 1993; Krawinkel et al. 1999; Caracciolo et al. 2016; Liang et al. 2019). Epidote analysis is generally considered a provenance tool of lesser value reflecting variable degrees of metamorphic overprint (Frei et al. 2004; Enami et al. 2004; Grapes and Hoskin 2004; Mange and Morton 2007; Liang et al. 2019). The epidote geochemical fingerprint has the potential, however, to release provenance information also of mafic rock types as shown in some cases (e.g., Nechaev and Isphording 1993; Krawinkel et al. 1999).

Framework component sandstone petrography is a traditional and well-established method (Krynine 1937; Dickinson 1970; Potter 1994; Weltje and von Eynatten 2004). Evaluation of light minerals and rock fragments in a sediment permits an initial discrimination of provenance (e.g., Dickinson and Suczek 1979; von Eynatten et al. 2003; Garzanti et al. 2007) and allows for a general insight into the nature of the sediment (Pettijohn et al. 1987). Supported by a statistical assessment, this presents information on source rock lithology and mixing of material supplied from different endmember sources.

Sample preparation and analysis

Samples were wet-sieved to remove grains < 63 µm. Bulk samples > 63 µm were investigated under a binocular microscope. Light and heavy minerals were separated using sodium polytungstate at 2.95 g/cm^3 by density separation. Both light and heavy mineral fractions 250–63 µm were mounted on microscopy slides in epoxy and grinded to ca. 35 µm. On each slide, 300 grains were point counted after the Gazzi-Dickinson point counting method (Ingersoll et al. 1984; Dickinson 1985) using a polarization microscope equipped with a Petrog SteppingStage. Grains > 250 µm were rare and examined under a binocular microscope and exemplary grains of the most common rock fragments were mounted in epoxy and prepared to be examined with a microscope. For pyroxene and epidote analysis, grains were handpicked under a binocular microscope from fractions of heavy mineral separates used in Huber et al. (2018a, b). Pyroxene and epidote major element geochemistry was measured using JEOL JXA-8530F Field Emission Electron Probe Microanalyzer at the Institut für Mineralogie at University of Münster. Minerals intergrown with the pyroxenes and epidotes were measured alongside. Acceleration voltage was at 15 kV, beam current at 10µA and spot size at 5 µm. Pyroxene end-members were calculated using the WinPyrox software (Yavuz 2013).

Results

Framework components

The non-clayey deposits encountered at Sites U1417 and U1418 are fine to medium sands and silts formed as turbidite overbank sediments (Expedition 341 Scientists 2014). Grains larger than medium sand are rare and represent less than 2% in most samples. Most samples consist of subrounded grains, subangular grains occur occasionally. The framework component composition of all samples mainly consists of quartz, feldspar, rock fragments, and accessory heavy minerals (electronic supplement Table 1). The distribution of framework components (QFL) classes the samples of both sites U1417 and U1418 as lithic sands and silts (Dott 1964), or as fLQ or fQL sands (Garzanti 2016). The sand-size fraction is dominated by quartz in all units (Fig. 3). The quartz content consists almost exclusively of monocrystalline quartz. Most of the feldspar is plagioclase, K-feldspar is scarce. Feldspars are relatively fresh with only minor sericitization, plagioclase shows polysynthetic twinning under the microscope (Fig. 4). The samples from the proximal Site U1418 contain more feldspar than those of the distal Site U1417 (Figs. 3, 5), the respective average framework modal compositions are $Q_{48}F_{17}L_{35}$ (U1418) and $Q_{47}F_{12}L_{41}$ (U1417). The main detrital phyllosilicate is biotite, followed by chlorite. The abundance of biotite is highest in the Miocene unit 6 at site U1417 (Fig. 2) and decreases up section at this site.

The most common rock fragments are argillite, aphanitic and micro-porphyric mafic rock fragments, fragments of intermediate to felsic intrusive rocks, sandstones, slates, schists, gneiss and metasiltstone (Figs. 6, 7; Expedition 341 Scientists 2014). Some of the sedimentary rock fragments show abundant opaque grains (Fig. 7g).

The sediments of the oldest Miocene samples recovered from unit VI (Fig. 2) have a very different composition from the younger strata. They contain a high proportion of coalified organic material, biotite and opaque, angular grains (Figs. 6f). Rock fragments, quartz and feldspar make up less than 5% of these sediments. Also, very different are the samples from the mass transport deposit at the base of the core retrieved from unit IV at Site U1418 (Jaeger et al. 2014). They are rich in black angular detrital grains of iron oxide > 0.25 mm.

Principle component analysis

The representation of the samples' framework composition in the QFL diagram (Fig. 5) illustrate that feldspar is slightly more abundant in the samples from Site U1418. This happens mostly at the expense of the lithic grains. Principle component analysis as applied to siliciclastic sedimentary rocks is a means to statistically underpin the assignation of compositional differences obtained by point counting (Vermeesh 2016; Fig. 8). Here, the vector loading of the principle input variables shows that the samples from Site U1418 are in fact characterised by a larger feldspar component whereas the samples from Site U1417 have higher amounts of rock fragments, and of fragments from sedimentary and metamorphic rocks, in particular (Fig. 8).

Implications of the framework petrography data

Petrographic framework component compositions are likely but not unequivocal guides to the tectonic setting of source areas. Original detrital signals may be obscured by mixing from different sources (Dickinson 1985; Garzanti 2016). Therefore, the QFL diagram does not unambiguously constrain the tectonic provenance of a sedimentary deposit but may serve as an initial graphical classification tool guiding

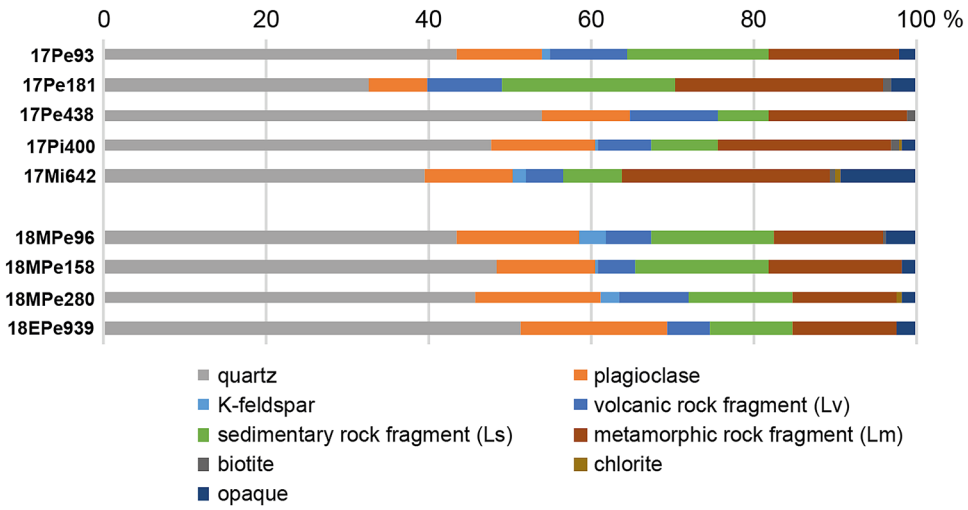

Fig. 3 Light mineral spectra of sites U1417 and U1418. Sedimentary, volcanic and metamorphic rock fragments correspond to the lithics categories Ls, Lv and Lm, respectively, of the Gazzi-Dickinson point counting method (Ingersoll et al. 1984)

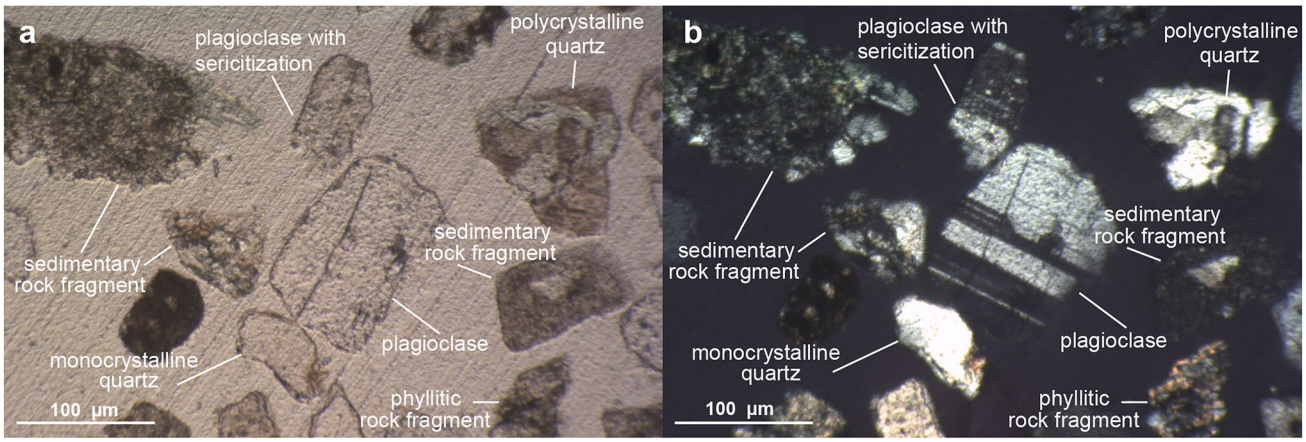

Fig. 4 Representative microphotographs of detrital grains from site U1417 and U1418. **a** Plane-polarized light, **b** cross-polarized light

further study which may combine the framework data with the more conducive single grain geochemical analysis of heavy minerals (von Eynatten et al. 2003; Garzanti 2016). Application of the classical QFL Dickinson diagram is most unerring when applied to detritus derived from active margins as it does not really allow for the consideration of anorogenic provenances including continental rifts (Garzanti 2016).

The classical Dickinson diagram does not include a specific active margin provenance. This provenance encompasses the magmatic arc and the recycled orogenic provenance types. As evidenced by the Andean cordillera orogen, climatic asymmetry leads to a magmatic arc provenance in sands derived from the western rain shadow pro-side of the mountain belt (Potter 1994; Garzanti et al. 2007). Contrastingly, erosion on the windward eastern and retro-side of the orogen is focused in fold and thrust belts exposing mainly Paleozoic siliciclastic sedimentary rocks results in sands with a recycled orogen provenance (Fig. 5; Potter 1994; Garzanti et al. 2007). In southern Alaska, the pro-wedge of the St. Elias orogen is located on the windward side, which also includes the fold and thrust belt on the Yakutat Terrane (Fig. 1; Trop and Ridgway 2007), thus combining both provenance types of Garzanti et al. (2007) on the southern, windward pro-side of the orogen.

We also note that sands derived from subduction complexes representing another leading edge provenance indicate a recycled orogen provenance (Fig. 1; Dickinson & Suczek 1979). On the windward side of the St. Elias orogen, the Chugach and Prince William terranes represent Mesozoic and Cenozoic subduction complexes, respectively (Fig. 1; Trop and Ridgway 2007). The provenance of the Surveyor Fan sediments can therefore be expected to potentially encompass both the classical magmatic arc and recycled orogen provenance, including subduction complexes. Concluding from this discussion, we will henceforth in this contribution consider the combined fields of magmatic arc and recycled orogen provenance as the realm of active margin provenance (Fig. 5).

The considered modification gives us confidence to use the QFL diagram in the analysis of the detrital compositions presented here as the active margin tectonic setting of sources in the St. Elias Orogen and the sink in the Surveyor Fan are well established since the seminal work by Plafker (1987). Compositional variations will rather reflect input from different sources in the exposed subduction complexes within the active margin St. Elias strike-slip orogen than changes of tectonic setting and overall provenance.

The studied samples from both sites have relatively similar average framework component compositions of $Q_{48}F_{17}L_{35}$ (U1418) and $Q_{47}F_{12}L_{41}$ (U1417) with the samples from site U1418 having slightly more feldspar (Figs. 1, 2, 3, 5, 8). In the QFL diagram of Dickinson et al. (1983; Fig. 5), the samples plot around the subduction complex provenance in the "recycled orogen" provenance field also including the clastic wedge provenance of Garzanti et al. (2007), all representing detritus derived through recycling of older orogenic detritus encompassing foreland basin systems, remnant ocean basins and collisional orogens (Fig. 1).

The analyzed samples from Sites U1417 and U1418 are predominantly fine sands and silts. They are poor in polycrystalline quartz. Considering relatively short transport distances from source to sink on the one hand, and predominantly robust subglacial to glaciofluvial transport processes on the other, it is likely that mechanically less stable polycrystalline quartz grains disintegrated to finer grain sizes along crystallographic domain boundaries. These finer quartz grains may have been additionally concentrated by sorting during transport. Original framework compositions may thus have been richer in fragments of polycrystalline quartz and rock fragments like chert and volcanic rocks (Figs. 5, 6), examples of which are contained in the

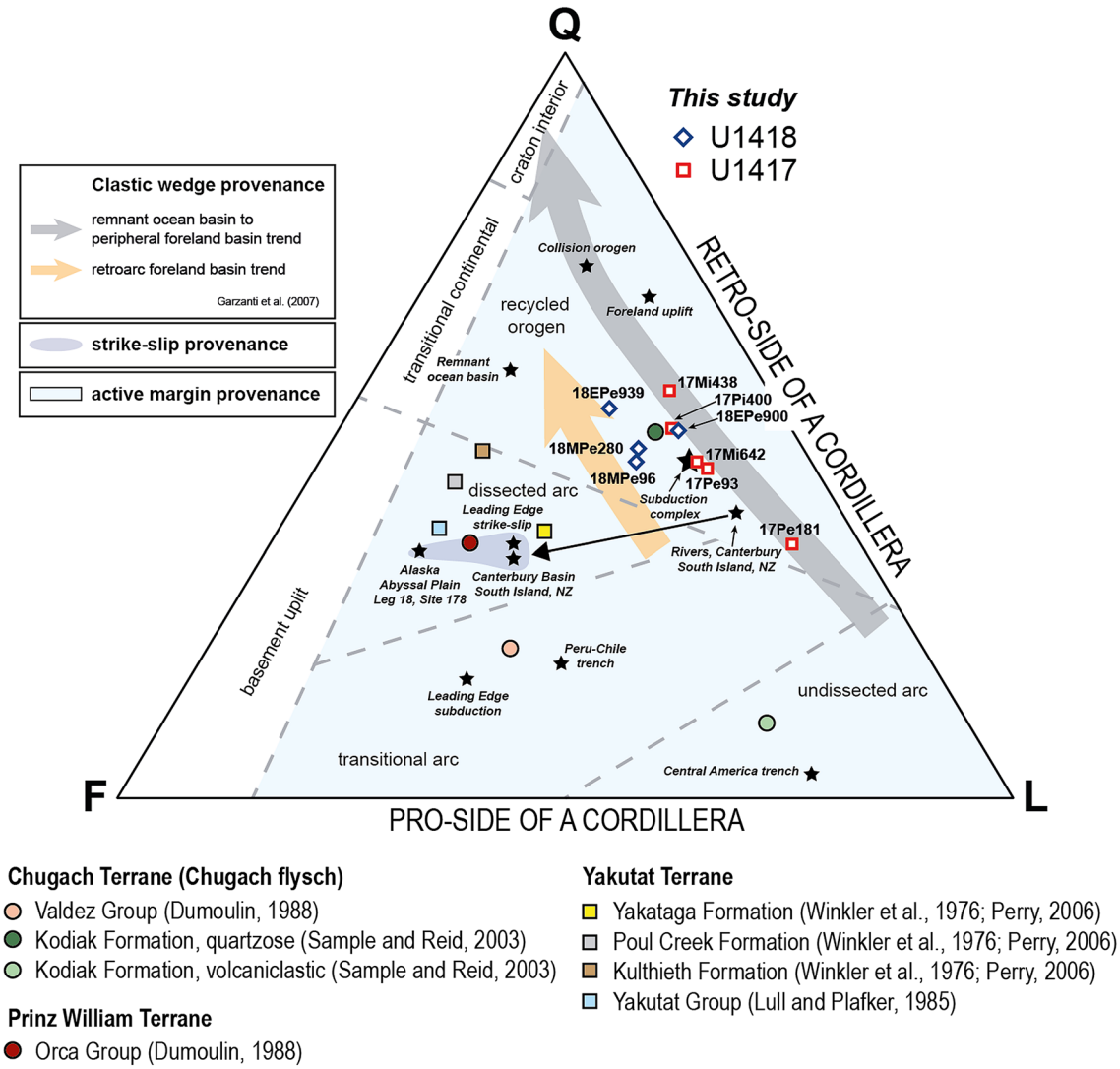

Fig. 5 QFL-diagram after Dickinson et al. (1983) with apices Q = quartz, F = feldspar and L = lithics showing the samples from site U1417 and U1418 plotting in the recycled orogenic provenance field, and averages of onshore reference samples (Fig. 1) from the literature. The sample 17Mi704 from unit VI (Figs. 2, 5f, 6) could not be plotted in this diagram because of the lack of grains of the respective groups. Black stars, average reference compositions; strike-slip regimes: Alaska Abyssal Plain sandstones, DSDP Leg 18, Site 178, middle Miocene (Hayes 1973); Leading edge strike-slip (Valloni and Maynard 1981); Canterbury Basin, and Canterbury rivers, South Island, New Zealand (Bender-Whitaker et al. 2018), the black arrow links the onshore river sand to the offshore turbidite sand compositions; subduction zones: Central America trench (Yerino and Maynard 1984); Leading edge subduction, Peru–Chile trench (Yerino and Maynard 1984; Thornburg and Kulm 1987); Remnant ocean basin, Bengal and Nicobar fans (Ingersoll and Suczek 1979); all others from Dickinson and Suczek (1979). Clastic wedge provenance and pro-side and retro-side indication according to Garzanti et al. (2007)

rare coarser fractions (Fig. 6). This would result in shifting the framework compositions of Sites U1417 and U1418 samples towards the magmatic arc provenance fields of the QFL diagram (Fig. 5). Conversely, the decrease of feldspar and increase of quartz from the older Yakutat Terrane units incorporated and exposed in the fold and thrust belt to the younger Surveyor Fan sediments (Fig. 1) may reflect the recycling process and loss of more labile components from the thrust belt into the ocean. However, both scenarios would not influence the general interpretation of an active margin provenance of the detritus.

The St. Elias orogen exposing Mesozoic and Cenozoic subduction complexes is presently a strike-slip orogen accommodating the northwestward movement of the Yakutat Terrane (Fig. 1; Elliott et al. 2010; Gulick et al. 2015). Available provenance data on strike-slip orogens were obtained from the deeper marine turbidite and contourite record (Hayes 1973; Valloni and Maynard, 1981; Bender-Whitaker et al. 2018) and plot in the dissected arc field of

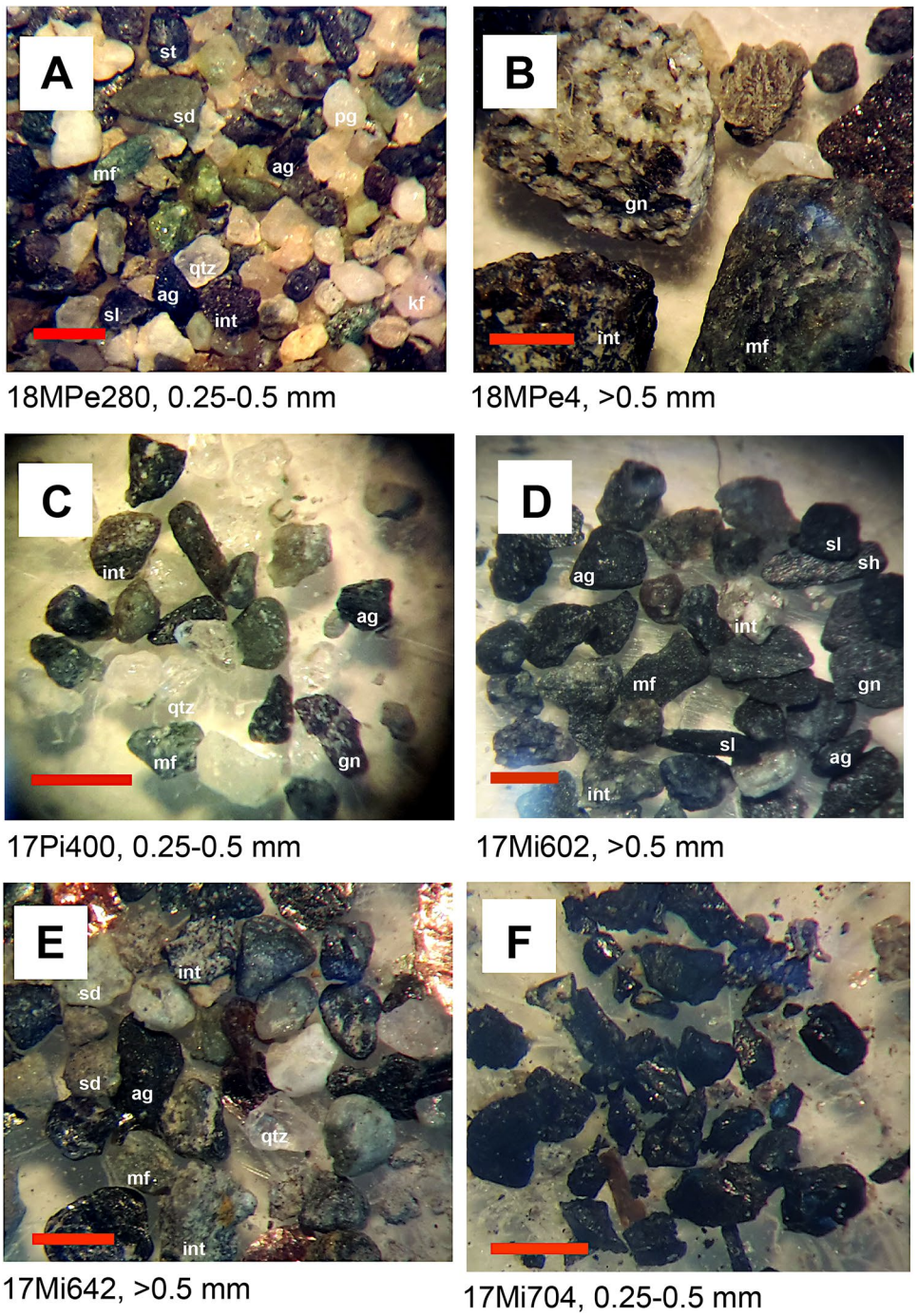

Fig. 6 Microphotographs of the silicate framework components in the grain fractions > 0.25 mm from site U1417 and U1418. ag, argillite; gn, gneiss; int, intrusive rock fragment; kf, K-feldspar; mf, mafic volcanic rock fragment; pg, plagioclase; sd, sandstone; sh, shist; qtz, quartz; sl, slate; st, shist; F, coalified organic fragments. Red scale bar represents 0.5 mm

the Dickinson diagram (Fig. 5). River sands from the Canterbury province east of the Southern Alps strike-slip orogen of New Zealand (Molnar and Dayem 2010) indicate a recycled orogen – clastic wedge provenance like the studied samples form the Gulf of Alaska (Fig. 5; Bender-Whitaker et al. 2018). In the New Zealand case, the significantly increased immaturity of the deep-sea deposits relative to the river sands is considered to be due to a mixture of the Canterbury River detritus with other material transported along shore and offshore by marine currents (Fig. 5; Bender-Whitaker et al. 2018).

The deep-marine sands recovered from the Gulf of Alaska abyssal plain by IODP Expedition 341 have a framework component composition very similar to the Canterbury river sands. An admixture of more immature detritus like in the New Zealand case is not observed for our samples but may have played a role in the genesis of the deposits recovered at DSDP Site 178 (Fig. 5; Hayes 1973). Glacial transport of detritus across the Yakutat shelf and onward transport to the

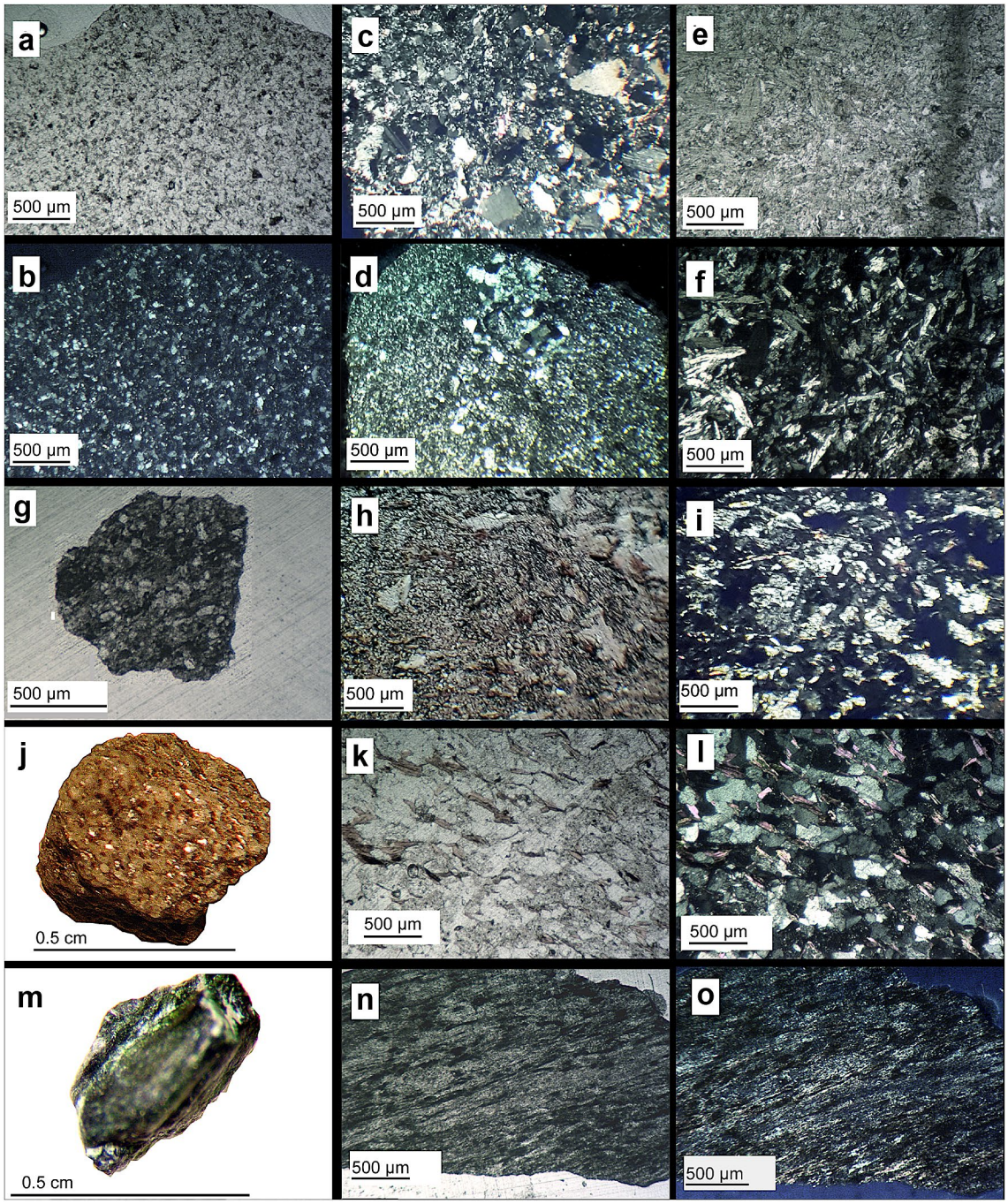

Fig. 7 Microphotographs of the common rock fragments in the sediments from sites U1417 and U1418. **a** Very fine-grained silt/mud stone with abundant quartz and feldspar, PPL (plane-polarized light); **b** XPL (cross-polarized light); same as A; **c** medium grained sandstone showing beginning recrystallization, XPL; **d** metasedimentary rock fragment showing beginning recrystallization and lineation, XPL; **e** metabasite showing chlorite formation; **f** XPL; same as **e**; **g** sedimentary rock fragment with abundant opaque grains, PPL; **h** PPL, metasedimentary grain showing chlorite formation and recrystallization, **i** XPL, same as h; **j** quartzofeldspathic schist showing lineation defined by biotite; **k** same grain as in j but cut and embedded into epoxy, PPL; **l** XPL, same as k; **m** greenschist facies metamorphic rock fragment; **n** same as m but cut and embedded into epoxy, PPL; **o** XPL, same as n

deep sea via trough mouth fans allowed for a direct transfer of material without admixture from other sources (Laberg and Vorren 2000; Gulick et al. 2015) and without significant intermediate storage (Clift et al. 2014). This also permits the interpretation of the studied samples as being derived from a strike-slip source exposing older subduction complexes. As the sand petrography does not allow for distinguishing between a subduction complex and a potential strike-slip

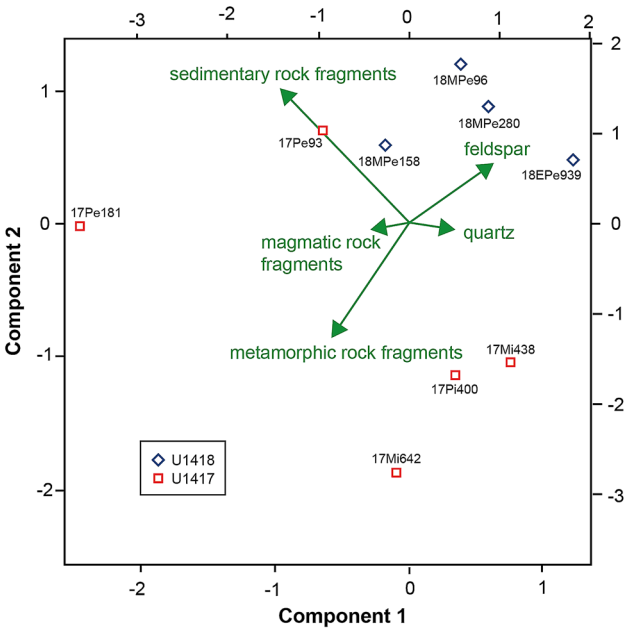

Fig. 8 Principal component analysis plot of the main framework components from samples of sites U1417 and U1418. Calculated with the *provenance()* software of Vermeesch et al. (2016)

provenance, we consider the general assignment of an active margin provenance helpful.

Onshore, the mature, quartzose part of the Kodiak Formation as part of the upper Cretacous Valdez Group turbidites has a QFL composition of $Q_{49}F_{15}L_{36}$ (Sample and Reid 2003; Fig. 5) similar to the studied samples. Rocks belonging to the younger part of the Kodiak Formation are richer in volcanic detritus with $Q_{10}F_{22}L_{68}$ and plot in the undissected arc field of the QFL diagram (Fig. 5) reflecting a change of their sources from the erosion of older, partly Proterozoic sources to increasing input of the contemporaneous Eocene arc (Sample and Reid 2003; Barefoot et al. 2020). Large parts of the Valdez Group are of a compositional maturity between the end-members of the Kodiak Formation, with an average framework composition of $Q_{20}F_{46}L_{34}$ (Fig. 5; Dumoulin 1988). The average composition of the Valdez Group resembles that of Modern trench sediments (Valloni and Maynard 1981; Thornburg and Kulm 1987) and falls in the transitional arc provenance field of the QFL diagram (Fig. 5).

Coeval and younger lithostratigraphic units exposed onshore in the St. Elias orogen fold and thrust belt, from the Upper Cretaceous Yakutat Group to the Miocene – Present Yakataga Formation, are richer in feldspar than rock fragments, and comparatively slightly enriched in quartz (Figs. 1, 5). They uniformly reflect a dissected magmatic arc provenance in the QFL diagram (Fig. 5). Their composition is also similar to Modern deep-sea sands derived from leading edge strike-slip orogens (Valloni and Maynard 1981), a finding that correlates directly with the tectonic setting of the St Elias orogen (Plafker et al. 1994; Elliott et al. 2010; Pavlis et al. 2012). Sands of Miocene age obtained by DSDP Leg 18 at Site 178 on the Alaska Abyssal Plain (Fig. 1; Hayes 1973) have a similar composition with $Q_{33}F_{49}L_{18}$, and thus have more feldspar and less rock fragments than the coeval and younger, and more quartz-rich, sands at Site U1417 and U1418 (Fig. 5).

Evaluation of the main rock fragments shows a difference between the samples from sites U1417 and U1418. The Miocene to Pliocene samples from site U1417 give higher numbers of metamorphic grains compared to the Pleistocene samples from site U1417 and site U1418. This corroborates the shipboard results of IODP Expedition 341 where macroscopic inspection of clast compositions > 2 mm in diameter gave a similar result (Figs. 6, 9). Furthermore, this is confirmed by principal component analysis (Vermeesch et al. 2016) showing all Pleistocene samples besides sample 17Pe181 to cluster in the topmost right corner of the plot while the Miocene to Pliocene samples plot towards the bottom right corner (Fig. 8). The rock fragment composition obtained in this study is consistent with a subduction complex – clastic wedge, active margin provenance and corroborates the results of Zuffa et al. (1980).

Heavy minerals, pyroxene and epidote

The heavy mineral spectra at both Sites U1417 and U1418 are characterized mainly by amphibole, pyroxene, epidote and garnet, in decreasing order of abundance. Biotite and chlorite represent scarce components (Huber et al. 2018b; Fig. 10). There are minor variations between sites. Epidote and amphibole are most abundant at Site U1417, and amphibole and pyroxene dominate at Site U1418. Garnet represents a minor but appreciable component (Fig. 10). The details of the geochemistry and provenance of amphibole and garnet have been presented by Huber et al. (2018b).

Pyroxene

Pyroxenes reflect the composition of the source rock and they form predominantly in mafic to intermediate magmatic lithologies and high-grade metamorphic rocks (Rösler 1984). Clinopyroxene is a common component in volcaniclastic sandstones derived from magmatic arcs (Cawood 1983; Nechaev and Isphording 1993). Clinopyroxene is, however, one of the most unstable detrital heavy minerals in sandstones (Morton and Hallsworth 2007). The geochemical composition of pyroxenes from Sites U1417 and U1418 allows for the classification based on major elements Mg, Ca and Fe (Morimoto et al. 1988).

The strongly predominant variety of pyroxene encountered in the studied samples is brown clinopyroxene

(Fig. 11a). Most pyroxene occurs intergrown with feldspar, mostly albite, pumpellyite and titanite (Fig. 11a). The most abundant pyroxene endmember at both sites is the clinopyroxene augite, with minor occurrences of diopside and hedenbergite (Fig. 12a; electronic supplement Table 2). All augite is relatively rich in aluminum (Appendix B). A few grains approaching the composition of the pyroxenoid wollastonite occur (Fig. 12a; Morimoto et al. 1988). Wollastonite is mostly derived from metamorphic calc-silicate lithologies and rarely from nephelenitic volcanic rocks (Pichler and Schmitt-Riegraf 1987).

Nisbet and Pearce (1977) established that the major element concentrations in pyroxenes reflect the plate tectonic setting of the mafic volcanic source rocks. In the triangular space of MnO-TiO_2-Na_2O, the pyroxenes of Sites U1417 and U1418 plot in a highly distributed pattern (Fig. 12b). There is no systematic variability in pyroxene composition between the two sites and between samples from different stratigraphic intervals (Fig. 12a, b). One can, however, state that the majority of sample compositions plot in the fields A, F and G, indicating a preferred provenance from volcanic arc and within plate alkalic basalts. The joint consideration of the predominance of green magnesiohornblende in the samples (Huber et al. 2018b) and the absence of olivine assigns the predominant brown clinopyroxenes to a convergent margin provenance according to Nechaev and Isphording (1993).

Epidote

Minerals of the epidote-zoisite group make up a large fraction of the heavy mineral spectra of site U1417 and U1418. All grains show a very similar geochemistry and consist predominantly of Fe bearing epidote (Table 1; electronic Supplement Table 3), zoisite is rare. Epidote is a heavy mineral which commonly forms during low-grade metamorphism of marls and other clay and carbonate bearing rocks, and of mafic rocks (Pichler and Schmitt-Riegraf 1987; Spiegel et al. 2002). Epidote also forms under medium pressure metamorphic conditions in mafic and intermediate magmatic rocks (Grapes and Hoskin 2004), and in high and ultrahigh pressure regimes in mafic magmatic and pelitic lithologies

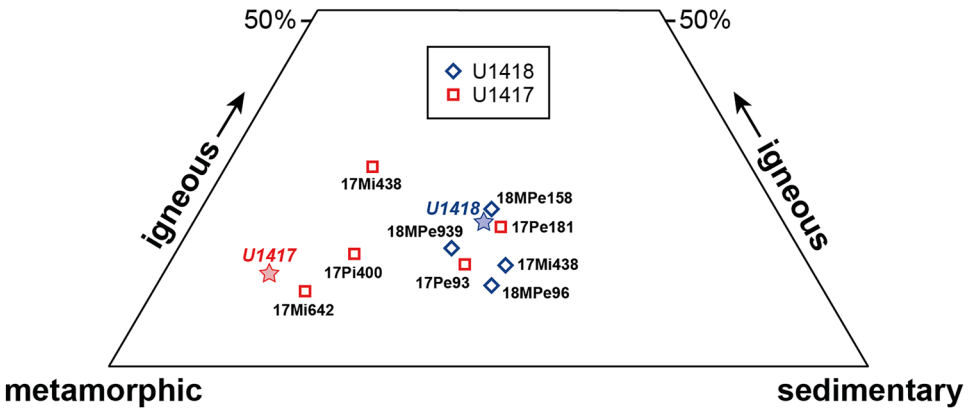

Fig. 9 Diagram showing the lithology of the rock fragments in samples from sites U1417 and U1418. The red and blue stars represent the average abundances of the main types of clasts larger than 2 mm in diameter at sites U1417 and U1418, respectively, as determined during on-board core description by IODP Expedition 341 Scientists (2014).

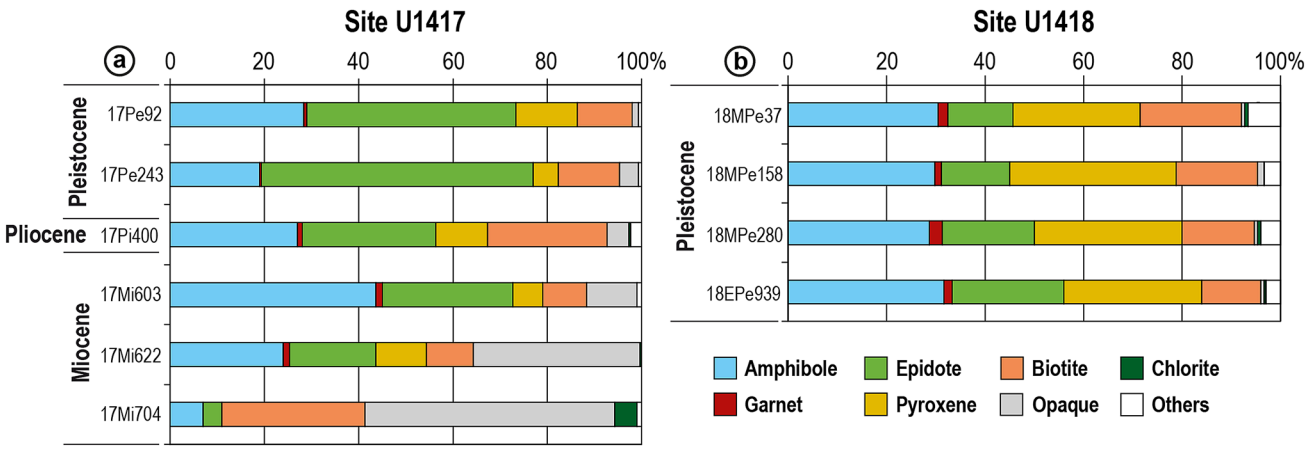

Fig. 10 Heavy mineral composition at the distal (**a**) and proximal (**b**) sites. *X* axis gives percentage of different minerals of the heavy mineral spectrum (modified from Huber et al. 2018b)

Table 1 Representative single grain geochemical analyses of epidotes from different samples from IODP 341 sites U1417 and U1418 in wt.%

Sample	Na_2O	MgO	SiO_2	Al_2O_3	K_2O	CaO	FeO	TiO_2	Cr_2O_3	MnO	Total
17Mi642	0.02	1.97	36.50	20.96	0.02	21.84	10.02	0.04	0.02	0.06	91.45
17Mi642	0.01	0.02	37.15	20.46	0.00	20.37	14.50	0.08	0.01	0.05	92.66
17Mi642	0.01	0.01	37.16	21.28	0.04	19.17	13.83	0.07	0.02	0.12	91.70
17Mi642	0.00	0.02	37.22	22.02	0.00	22.67	12.84	0.06	0.08	0.17	95.08
17Mi642	0.01	0.02	37.23	21.44	0.00	22.86	13.56	0.10	0.04	0.20	95.46
17Pi400	0.04	0.01	36.84	19.32	0.00	21.58	16.20	0.00	0.01	0.00	94.00
17Pi400	0.03	0.20	37.30	21.33	0.00	22.11	14.04	0.24	0.00	0.11	95.35
17Pi400	0.00	0.11	37.37	21.28	0.01	21.93	13.66	0.08	0.00	0.17	94.61
17Pi400	0.00	0.05	37.40	21.38	0.01	22.15	13.81	0.00	0.01	0.26	95.08
17Pi400	0.03	0.04	37.49	22.61	0.00	20.56	13.03	0.09	0.00	1.05	94.90
17Pe93	0.07	1.98	34.88	23.69	0.03	17.19	14.88	0.00	0.00	0.77	93.50
17Pe93	0.00	0.03	35.34	15.31	0.02	24.08	9.73	10.27	0.02	0.08	94.88
17Pe93	0.00	0.06	36.88	21.26	0.02	22.73	13.03	0.00	0.00	0.27	94.25
17Pe93	0.01	0.01	37.17	21.52	0.00	21.40	13.36	0.08	0.00	0.12	93.67
17Pe93	0.00	0.04	37.18	20.73	0.00	22.64	14.38	0.15	0.00	0.07	95.19
18MPe280	0.00	0.06	36.49	22.28	0.03	23.58	11.41	0.15	0.02	0.28	94.30
18MPe280	0.02	0.09	36.50	18.88	0.01	22.87	12.27	4.29	0.01	0.11	95.05
18MPe280	0.02	0.05	36.81	20.57	0.02	22.64	14.78	0.17	0.00	0.18	95.24
18MPe280	0.04	0.02	36.95	20.72	0.05	22.52	13.94	0.20	0.03	0.13	94.59
18MPe280	0.01	1.93	37.00	22.38	0.00	20.94	12.47	0.25	0.04	0.18	95.19

(Enami et al. 2004). It may also be the product of the metasomatic alteration of pyroxene, amphibole and anorthite in magmatic rocks (Pichler and Schmitt-Riegraf 1987). The geochemistry of epidote minerals is highly variable. It is controlled by temperature, pressure, oxygen fugacity (fO_2), and bulk rock composition. In metamafic rocks, epidote

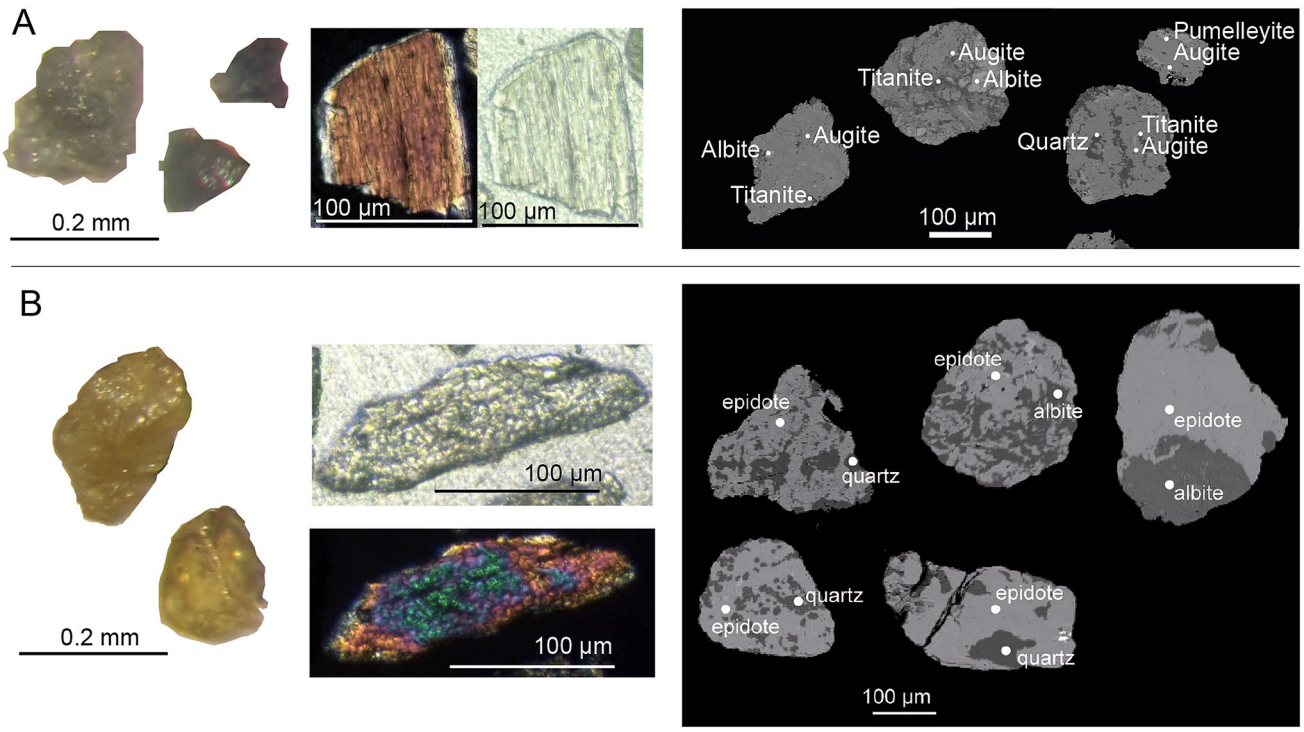

Fig. 11 Representative binocular microscope, thin section and microprobe images of **a** augite intergrown with titanite and/or quartz and **b** epidote intergrown with albite, titanite and/or quartz from the site U1417 and U1418 samples

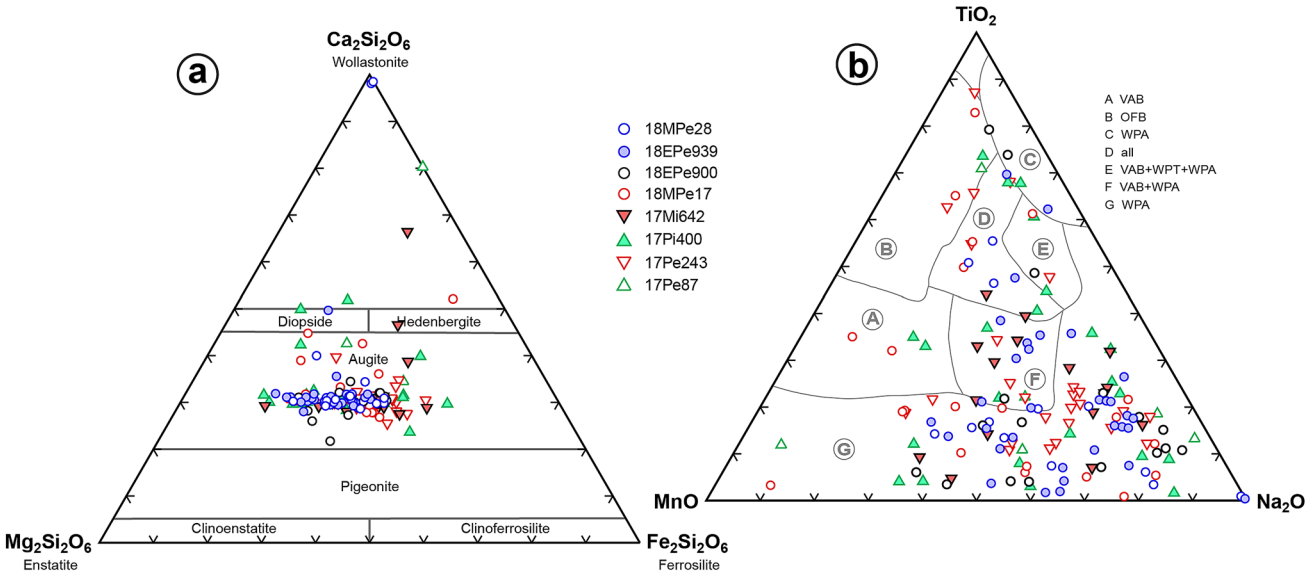

Fig. 12 Geochemical composition of pyroxene from site U1417 and U1418. **a** Major element composition of pyroxene and the pyroxenoid wollastonite according to Morimoto et al. (1988). **b** Composition of pyroxene according to Nisbet and Pearce (1977) showing no trend in correlation of sampling depth and stratigraphic position to tectonic setting. **a** volcanic arc basalts (VAB); **b** ocean floor basalts (OFB); **c** within plate alkalic basalts (WPA); **d**, all; **e**, volcanic arc basalts + within plate tholeiitic basalts + within plate alkalic basalts (VAB + WPT + WPA); **f**, volcanic arc basalts + within plate alkalic basalts (VAB + WPA); G, within plate alkalic basalts (WPA)

shows a tendency to higher Fe (Enami et al. 2004). Epidote is unstable under burial conditions, but less so than clinopyroxene (Morton and Hallsworth 2007; Garzanti et al. 2020).

Most grains of the epidote group at Sites U1417 and U1418 are intergrown with albite or quartz (Fig. 12b). There is no systematic variability in epidote composition with time of deposition or between sites. The amount of epidote, however, varies between the two sites. At the distal site, the epidote content of the heavy mineral fraction rises from ca. 16% in the Miocene to 58% in the Pleistocene sediments (Huber et al. 2018b). Within the Pleistocene samples from the proximal site (U1418), epidote content is relatively constant at ca. 22% to ca. 18% (Huber et al. 2018b).

The X_{Fe} value of epidote is a measure of metamorphic grade and increases towards lower grades (Grapes and Hoskin 2004; Enami et al. 2004). X_{Fe} is calculated as $[Fe^{3+}/(Al+Cr+Fe^{3+}+Mn^{3+})]$(Enami et al. 2004). The X_{Fe} values from both sites are rather similar and range between 0 and 0.9 (Fig. 13). The modes of the individual and combined distributions are at ca. 0.5 (Fig. 13a). The sample averages cluster between X_{Fe} values of 0.4 and 0.5 (Fig. 13b). These are relatively high and indicative of metamorphic conditions of relatively low temperatures and low to intermediate pressures (Enami et al. 2004). The less abundant low X_{Fe} values indicate that some epidote had been derived from high-pressure/high-temperature metamorphic terrains (Fig. 13).

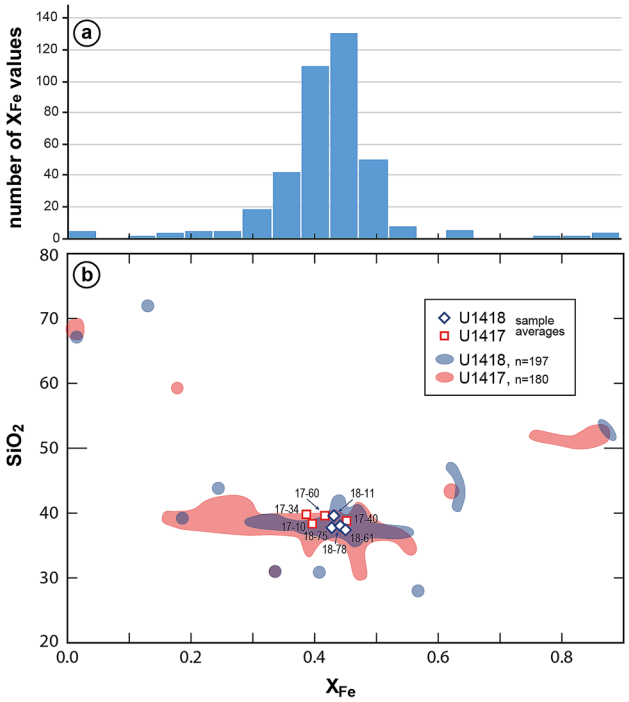

Fig. 13 X_{Fe} values of detrital epidote, combined from sites U1417 and U1418. X_{Fe} calculated according to Enami et al. (2004). **a** Histogram of X_{Fe} values from both sites; **b** X_{Fe} vs SiO_2 diagram

Implications of the pyroxene and epidote data

Augite is the predominant pyroxene in the studied samples (Fig. 12a). It is the most abundant mafic mineral in calcalkaline and tholeiitic magmatic rocks (Pichler and Schmitt-Riegraf 1987). The geochemical characteristics of the analyzed mineral grains assign their original formation predominantly to a convergent (active) margin provenance (Fig. 12b). A potential source lithology may have been the metabasite belt at the southern margin of the Chugach Metamorphic Complex (Bruand et al. 2011; Gasser et al. 2011). The studied epidote minerals have geochemical characteristics indicating an origin in a high temperature–low-pressure metamorphic belt like the Chugach Metamorphic Complex.

$^{40}Ar/^{39}Ar$ ages on hornblende obtained from several samples from Sites U1417 and U1418 group mainly at ca. 145–133 Ma (very early Cretaceous), and between 55 and 37 Ma (Eocene; Huber et al. 2018b). Detrital zircon U–Pb age distributions from Site U1417 and U1418 sediments have a pronounced maximum at 60 to 50 Ma (Paleocene–Eocene; Huber et al. 2018a). In the evolving St. Elias orogen, Paleocene-Eocene time saw the intrusion of the Sanak-Baranof Plutonic Belt and the metamorphic overprint of the Chugach Metamorphic Complex caused by ridge subduction (Fig. 1; Sisson et al. 2003; Farris and Paterson 2009). Both lithotectonic units are very likely sources of pyroxene and epidote even though no age information on both minerals is available. The Sanak-Baranof Plutonic Belt and the Chugach Metamorphic Complex with the metabasite belt at its southern margin probably sourced the bulk of the pyroxenes and epidotes. The Chugach Metamorphic Complex and the metabasite belt have already been determined as the major source of hornblende and garnet in the sediments of Sites U1417 and U1418 (Huber et al. 2018b). Rocks of the Early Cretaceous Chisana arc on the Wrangellia Terrane may have been additional sources (Trop and Ridgway 2007).

The combination of our new pyroxene and epidote data with the already available heavy mineral data of Huber et al. (2018b) allows for the consideration of overall heavy mineral compositions in terms of likely tectonic setting of the sources (Fig. 14; Garzanti et al. 2007). The abundances as displayed in A – &tHM – O + P + S (amphibole—all other heavy minerals – olivine + pyroxene + spinel) space emphasize the derivation of the minerals from metamorphic terrains of greenshist to amphibolite facies grade (Fig. 14) corresponding to the axial-belt orogenic provenance of Garzanti et al. (2007).

As particularly pyroxene is a very unstable mineral during transport and burial significant recycling of mineral grains seems unlikely. The mentioned sources must have been contributing detritus more or less directly to the evolving Surveyor Fan.

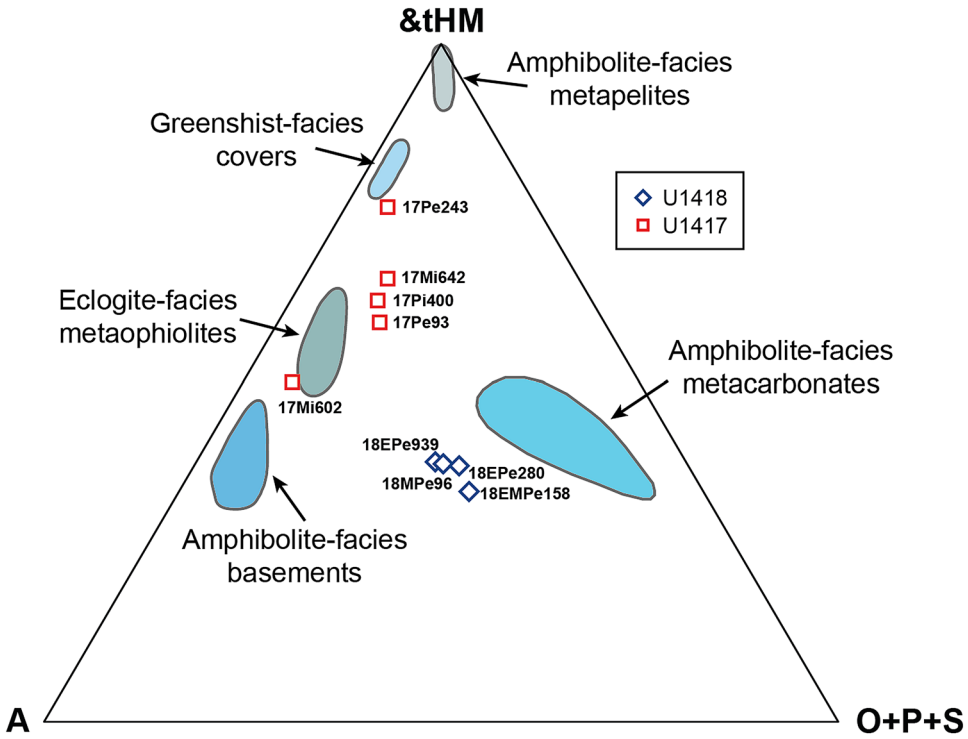

Fig. 14 Triangular diagram after Garzanti et al. (2007) showing the heavy mineral composition of site U1417 and U1418 sediments. A = amphibole, &tHM = all other transparent heavy minerals, O + P + S = olivine + pyroxene + spinel. Heavy mineral data from this study and Huber et al. (2018b)

Discussion and Interpretation

Large-scale provenance

The sands and silts recovered at Sites U1417 and U1418 are relatively well-sorted quartz-intermediate deposits of turbidity currents building up the Surveyor deep-sea fan on the Gulf of Alaska sea floor (Plafker et al. 1994; Gulick et al. 2015). They range in age from the middle Miocene to the Pleistocene (Fig. 2; Jaeger et al. 2014). The sediments from both sites have similar overall compositions. In terms of light mineral framework components, they are rich in feldspar and rock fragments and have an active margin orogen provenance directly connected to the adjacent accretionary St Elias orogen (Figs. 2, 5).

Joint consideration of petrographic characteristics, U–Pb age data on detrital zircons (Huber et al. 2018a) and detailed geochemical data on the heavy minerals amphibole and garnet (Huber et al. 2018b), and of pyroxene and epidote (this contribution) allows to identify the ultimate sources of the detritus. These are the Sanak-Baranof Plutonic Belt and the Chugach Metamorphic Complex (Fig. 2; Huber et al. 2018a,b) now exposed in subduction complexes in an active margin orogen, with significant contributions from the axial metamorphic belt (Figs. 5, 14).

Partial cycling of original detritus through intermediate storages represented by the Kulthieth, Poul Creek and Yakataga formations exposed in the St. Elias fold and thrust belt is likely given the syn-orogenic control on all Cenozoic deposits on the mainland and the Gulf of Alaska abyssal plain (Plafker et al. 1994; Enkelmann et al. 2008; Perry et al. 2009). The ubiquitous and abundant presence of unstable clinopyroxene indicates, however, that destruction of labile minerals during recycling and transport has been a minor factor.

Detailed observations on provenance

Framework components

Considering the temporal evolution of provenance, a major change occurred in the late Miocene, from mainly coalified organic material and mica to abundant quartz, feldspar and rock fragments (Site U1417, Fig. 2). This implies a modification of sediment transport mechanism on- and/or offshore, and/or a change in erosion patterns in the potential source areas. As it predates the onset of glaciation (Reece et al. 2011), tectonic processes are most likely to have triggered the change in sediment composition by changes in the loci of erosion and avenues of sediment dispersal.

The abundance of coalified organic material in Unit VI (Fig. 2, 6f) implies coal bearing strata to have fed most of these deposits. Jaeger et al. (2014) suggest the coaliferous alluvial and shallow marine Kulthieth Formation (56–33.9 Ma) on the Yakutat terrane as main source. Today, this formation is exposed in the fold and thrust belt on the Yakutat Terrane which belongs to the Cenozoic subduction complex at this margin (Trop and Ridgway 2007). Due to the northwestward movement of the Yakutat terrane since 10 Ma, these rocks must have been located further southeast during deposition of the site U1417 sediments. Geochemical and biomarker analyses of the coals from the Kulthieth Formation and the site U1417 sediments confirm the origin of the material (Childress et al. 2013). The Kulthieth, Poul Creek and Yakataga formations have been found to differ in the biomarkers of their organic carbon (Childress and Ridgway 2014). For now, the source region of these sediments cannot be further specified but a Yakutat terrane source is likely.

The Yakataga Formation, in turn, has been deposited coevally with the Surveyor Fan sediments. It has been suggested to be sourced by two or more sources, most likely the Chugach-Prince William terrane and the Poul Creek and Kulthieth formations on the Yakutat Terrane (Plafker et al. 1994; Enkelmann et al. 2008; Perry et al. 2009). This is in line with erosion and transport of material also from the Kulthieth Formation via the Yakataga Formation or directly into the precursor of today's Surveyor Fan at ca. 11 Ma.

Sediment accumulation rates increased in the Gulf of Alaska between 9.87 and 9.47 Ma with the initiation of Surveyor Fan turbidite deposition (Rea and Snoeckx 1995). At the same time, unit VG (Fig. 2; sample 17Mi642, ca. 8.5–9.5 Ma) has been deposited at Site U1417. This unit has been found to be very likely sourced by the Chugach Metamorphic Complex (Huber et al. 2018a,b). The high amount of metamorphic rock fragments (Fig. 9, sample 17Mi642) supports this finding.

Because of the Miocene position of site U1417 further to the southeast, an efficient transport system is required to feed material into the Site U1417 region. Seismic data suggest transport of material from sources to the north into the precursor of the Surveyor Fan (Stevenson and Embley 1987). Exhumation rates of the northeastern side of the St. Elias Syntaxis were extremely high at ca. 10 Ma and a fluvial system is considered to have existed, effectively eroding and exporting the material out of the orogen (Enkelmann et al. 2017). A link between these two inferred fluvial systems might explain the early input from the St. Elias orogen into the Surveyor Fan precursor. The change in sediment composition from mica and organic rich material to higher amounts of heavier minerals and rock fragments also implies a change to a higher energy transport regime.

While detailed analysis of heavy minerals from the Miocene to Pleistocene sediments from sites U1417 and U1418 shows changes with depositional age (Huber et al. 2018b), the light mineral composition is uniform from late Miocene onwards for Site U1417 and for the Pleistocene at the proximal Site U1418. This is not surprising as light mineral analysis has already been found to be less discriminative provenance indicator than heavy mineral analysis (von Eynatten et al. 2003). In fact, many lithologies at the southern Alaskan continental margin provide high amounts of quartz and feldspar to the erosional systems (Bruand et al. 2014; Hudson and Plafker 1982). Biotite, quartz and plagioclase have been found to make up 90% of the central part of the schist zone of the Chugach Metamorphic Complex (Hudson and Plafker 1982).

Considering framework component compositions together with transport and sorting effects, all samples from site U1417 and U1418 essentially imply an active margin orogen source. The slightly higher feldspar content at Site U1418 might result from the more proximal position of this site relative to the continental sediment routing systems to the Surveyor Fan. Plutons along the Southern Alaskan continental margin in the eastern and central Chugach Metamorphic Complex show granitoid to tonalitic compositions, while plutons further east tend to have less quartz and more plagioclase, showing a more gabbroic composition (Bradley et al. 1993).

Site U1418 sediments have been found to be sourced through the Bering-Bagley glacial system (Fig. 1) whereas site U1417 was sourced from a much wider part of the orogen with longer transport paths (Dunn et al. 2017; Huber et al. 2018a,b), being in line with the differences in feldspar abundance. K-feldspar is a minor component present of all samples (0–3%). In the potential source region, K-feldspar has only been found in appreciable amounts in the sedimentary units of the Cretaceous units in the Yakutat area, on the Chugach terrane (Zuffa et al. 1980). On average they show 5% K-feldspar with values ranging between 0.65 and 14.5% (Zuffa et al. 1980). K-feldspar is absent in the amphibolite facies schists of the Chugach Metamorphic Complex while it is present in the migmatites in the central parts of the complex (Hudson and Plafker 1982). The low abundance of K-feldspar matches a Chugach and Yakutat terrane provenance but cannot be used to further define the provenance of the sediments.

The rock fragment spectra of the samples show a slight decrease of metamorphic grains from the Miocene to the Pliocene and even lower numbers of metamorphic grains in all Pleistocene samples from both sites. This indicates an increased derivation during the Pliocene of material from the non-metamorphic and low-grade metamorphic units now exposed in the near-shore region on the Yakutat terrane. Metapelites, metagraywacke, shists and migmatites are the main lithologies of the inboard Chugach Metamorphic Complex whereas greenschist facies phyllites occur outside of it (Bruand et al. 2014). The phyllites have a uniform petrography of chlorite, epidote, muscovite, plagioclase, quartz and biotite (Bruand et al. 2014).

The trend of increasing input from the areas closer to the coast with younger depositional age and during increasing degrees of glaciation and advancing glaciers has also been indicated by zircon U/Pb age data (Huber et al. 2018a). The overall decrease of metamorphic rock fragments from site U1417 to site U1418 reflected in this study has also been observed regarding rock fragments > 2 mm by IODP 341 Scientists (2014; Fig. 9).

Heavy minerals

Pyroxene is the most abundant ferromagnesian heavy mineral with a relatively uniform composition at Sites U1417 and U1418. Augite appears together with pumpellyite, titanite, albite and quartz which is typical for the pumpellyite facies (Coombs 1989) supporting direct input to all samples from the low-grade metamorphic rocks of the Chugach Metamorphic Complex. Some of this detritus may also have been supplied indirectly by recycling through the Miocene-Present Yakataga Formation (Plafker et al. 1994; Enkelmann et al. 2008) now exposed in the fold and thrust belt on the western Yakutat Terrane (Fig. 1b). The higher amount of pyroxene present in the sediments at the proximal site is again in line with a derivation mainly from the Chugach Metamorphic Complex via the Bering-Bagley and Malaspina glaciers and the Icy Leg channel (Fig. 1).

Epidote together with albite and quartz are important components of the metabasalt belt cropping out along the southern border of the Chugach Metamorphic Complex (Lull and Plafker 1985; Bruand et al. 2011). The higher abundance of pyroxene at the distal site from the Miocene to the Pliocene and especially in the Pleistocene is in line with an increasing input from this part of the orogen. In the Pleistocene, the mineral associations containing epidote and pyroxene match input from the lower-grade metamorphic rocks on the Yakutat terrane to the proximal Site U1418, and from the higher-grade Chugach Metamorphic complex to the distal Site U1418. Increased erosion rates and changes and differences in the petrographical composition of the deposits are in line with the contemporaneous advance and expansion of the glaciers covering the St. Elias orogen.

The suites of transparent heavy minerals of both sites show marked differences (Fig. 14). The site U1417 sediments are rich in amphibole, plotting in the typical area for a clastic wedge or greenschist facies to amphibolite facies axial-belt provenance according to Garzanti et al. (2007). The site U1418 sediments show higher amounts of epidote, placing them in the middle of the unroofing trend typical for

undissected arc settings Garzanti et al. (2007). This underlines the difference in provenance of the two sites being fed by different glacial systems and different parts of the orogen.

Considerations of climate and tectonics

The data obtained from sands and silts recovered by IODP Expedition 341 by various studies yield a consistent scenario for the development of tectonic-climate interactions at the southern Alaska margin. Thermochronological data obtained from the distal Site U1417 (Fig. 1) indicate that rapid, strong, and deep-seated exhumation happened between ca. 11 and 8 Ma (Dunn et al. 2017). Site U1418 and more proximal sites on the southern Alaska shelf record detritus input from the general St. Elias orogen and minor mixing on the glaciated margin since 1.2 Ma (Dunn et al. 2017; Huber et al. 2018a). Depending on model parameters and the applied age model, exhumation rates could have been as high as between 2.6 and 5 km/My (Dunn et al. 2017; Huber et al. 2018a). Considering the area underneath the Bagley Ice Field, through which most of the detritus at Site U1418 has been delivered, ca. 3–4 km of rock exhumation has taken place since 4–3 Ma (Dunn et al. 2017).

A general and potentially abrupt change in provenance in response to the intensification of glaciation at the mid-Pleistocene transition is not reflected in our data. Heavy mineral spectra, the compositions of amphibole, garnet, pyroxene and epidote as well as the zircon age data and the framework petrography are uniform throughout the Pleistocene stratigraphy (Huber et al. 2018a, b). This implies that climatic changes at the mid-Pleistocene transition did not cause significant changes in the principal areas under erosion, with glaciers eroding most of the material in their topographically predefined positions (Gulick et al. 2015). Similar uniform heavy mineral spectra and amphibole and garnet geochemical compositions have been observed also in the middle Pleistocene to Holocene sediments from sites U1419 and U1420 (Drewer 2016).

Examination of the silt-sized fraction (15–63 µm) of surficial sediments collected throughout the Gulf of Alaska and of the mid-Pleistocene sediments recovered by IODP Expedition 341 confirms the establishment of persistent erosion centers controlled by the pronounced interaction of tectonics and the glacial cover at least since the mid-Pleistocene transition (Jaeger et al. 2017; Penkrot et al. 2017 2018). Since the mid-Pleistocene transition at ca. 0.7 Ma, sediment sources are inferred to have been situated within a narrow band of ~ 200–1500 m elevation that coincides with the last glacial maximum equilibrium-line altitude (ELA) range during the mid-late Pleistocene, feeding sediments of relatively homogenous composition into the Gulf of Alaska through the Bering-Bagley and Malaspina glacial systems (Jaeger et al. 2017; Penkrot et al. 2017). The age information obtained from detrital minerals (Dunn et al. 2017; Huber et al. 2018a,b) of Surveyor Fan sediments as well as the light mineral component and heavy mineral distributions do not provide evidence for the mass redistribution after the mid-Pleistocene transition having had a significant effect on the stress regime of the orogen.

The multiproxy dataset on detrital U–Pb zircon age and Hf isotope data, and Ar–Ar age data on detrital amphibole together with framework component petrographic and single-grain geochemical data on amphibole, garnet, pyroxene and epidote offers consistent constraints on the ultimate source lithologies of the Surveyor Fan sediments. The principal sources since the late Miocene are the Chugach Metamorphic Complex and the Paleocene-Eocene Sanak-Baranof plutonic belt (Fig. 1), both of which are included in the Mesozoic subduction complex comprising the Prince William and Chugach terranes (Fig. 1). This detritus has been reworked at least partly through the sedimentary formations deformed in the Cenozoic fold and thrust belt on the Yakutat Terrane as the lower-grade and non-metamorphic rocks closer to the coast have been incorporated into the mass redistribution processes (Fig. 1; Huber et al. 2018a,b). Increasing glaciation at the mid-Pleistocene transition did not result in a significant change in the provenance, implying the drainage area and glaciers to have been nested in their topographically defined positions throughout this combined tectonic-climatic evolution (Gulick et al. 2015; Huber et al. 2018a, b).

Conclusion

The framework component composition of the sands and silts of Miocene to Pleistocene age recovered by IODP Expedition 341 in the Gulf of Alaska uniformly reflects the expected active margin provenance most likely connected to erosion of exposed subduction complexes representing the Chugach and Prince William terranes. Pyroxene and epidote also have a consistent geochemical composition in all Miocene to Pleistocene samples. This indicates a persistence of sources and provenance. Detailed analysis of pyroxene and epidote grains indicates the Sanak-Baranof Plutonic Belt, the Chugach Metamorphic Complex and the metabasite belt at its southern border as the main sources of pyroxene and epidote, and the low-grade metamorphic rocks on the Yakutat terrane as additional sources. Increasing amounts of epidote from the Miocene to the Pleistocene at the distal site are in line with progressive input from the metabasite belt at the southern edge of the Chugach Metamorphic Complex. This confirms a general shift in erosion from the central part of the Chugach Metamorphic Complex to the southern flanks of the orogen with increasing glaciation.

The higher amount of epidote in the Pleistocene sediments from the proximal site is in line with higher contributions from the formations exposed in fold and thrust belt on the western Yakutat terrane. The different positions of the sites in relation to the Surveyor Fan tributary system very likely caused different parts of the orogen to contribute variable amounts of material. This has also been found in zircon and other heavy mineral data (Dunn et al. 2017; Huber et al. 2018a,b). In general, framework component, pyroxene and epidote data as well as the abundance and origin of different larger rock fragments are in line with a dominant contribution from relatively near-shore sources in the Pleistocene. This concurs with the increasing glaciation since the Miocene to have shifted erosion towards the coast, a trend enhanced by the onset of Northern Hemisphere glaciation in the Pleistocene.

Supplementary Information The online version contains supplementary material available at https://doi.org/10.1007/s00531-021-02025-9.

Acknowledgements This study was funded by German Research Foundation (DFG) Grant BA 1011/43-1 and -2 and is part of the research subsequent to IODP Expedition 341 Southern Alaska Margin. We thank M. Dröllner, Münster, for helping to process the samples and J. Berndt and B. Schmitte, Münster, for assistance with acquiring the microprobe data. We appreciate the comments of P. Castillo, Münster, on an early version of this manuscript. The reviews by Sergio Andò, Milan, and Ken Ridgway, West Lafayette, IN, were very helpful and are highly appreciated.

Funding Open Access funding enabled and organized by Projekt DEAL.

References

Andò S, Morton A, Garzanti E (2014) Metamorphic grade of source rocks revealed by chemical fingerprints of detrital amphibole and garnet. In: Scott RA, Smyth HR, Morton AC, Richardson N (eds) Sediment provenance studies in hydrocarbon exploration and production. Geological Society of London, Spec Publ 386:351–371

Arkle JC, Armstrong PA, Haeussler PJ, Prior MG, Hartman S, Sendziak KL, Brush JA (2013) Focused exhumation in the syntaxis of the western Chugach Mountains and Prince William Sound, Alaska. Geol Soc Am Bull 125:776–793

Barefoot J, Nadin ES, Newberry RJ, Camacho A (2020) Rock and age relationships within the Talkeetna forearc accretionary complex in the Nelchina area, southern Alaska. Can J Earth Sci 57:709–724

Bender-Whitaker C, Marsaglia KM, Browne GH, Jaeger JM (2018) Sedimentary processes and sequence stratigraphy of a Quaternary siliciclastic shelf-slope system: insights from sand provenance studies, Canterbury Basin, New Zealand. In: Ingersoll RV, Lawton TF, Graham SA (eds) Tectonics, sedimentary basins, and provenance: a celebration of william R. Dickinson's Career. Geological Society of America Spec Pap 540:1–38.

Berger AL, Gulick SPS, Spotila JA, Upton P, Jaeger JM, Chapman JB, Worthington LA, Pavlis TL, Ridgway KD, Willems BA, McAleer RJ (2008) Quaternary tectonic response to intensified glacial erosion in an orogenic wedge. Nat Geosci 1:793–799

Bergmann F, Schwenk T, Spiess V, France-Lenord C (2020) Middle to late pleistocene architecture and stratigraphy of the lower bengal fan—integrating multichannel seismic data and IODP expedition 354 results. Geochem Geophys Geosyst 21: e2019GC008702

Bootes N, Enkelmann E, Lease R (2019) Late miocene to pleistocene source to sink record of exhumation and sediment routing in the gulf of alaska from detrital zircon fission-track and U-Pb double dating. Tectonics. https://doi.org/10.1029/2019TC005497

Bradley DC, Haeussler PJ, Kusky TM (1993) Timing of early Tertiary ridge subduction in southern Alaska. In: Dusel-Bacon C, Till AB (eds) Geologic studies in Alaska by the US Geological Survey. US Geol Surv Bull 2068:163–177

Bradley DC, Kusky TM, Haeussler PJ, Goldfarb RJ, Miller ML, Dumoulin JA, Nelson SW, Karl SM (2003) Geologic signature of early Tertiary ridge subduction in Alaska. In: Sisson VB, Roeske SM, Pavlis TL (eds) Geology of a transpressional orogen developed during ridge-trench interaction along the North Pacific margin. Geol Soc Am Spec Pap 371:19–49

Bruand E, Gasser D, Bonnand P, Stuewe K (2011) The petrology and geochemistry of a metabasite belt along the southern margin of Alaska. Lithos 127:282–297

Bruand E, Gasser D, Stüwe K (2014) Metamorphic P-T conditions across the Chugach Metamorphic Complex (Alaska)—a record of focussed exhumation during transpression. Lithos 190–191:292–312

Bruhn RL, Pavlis TL, Plafker G, Serpa L (2004) Deformation during terrane accretion in the Saint Elias orogen. Alaska Geol Soc Am Bul 116:771–787

Bruns TR (1983) Model for the origin of the Yakutat terrane, an accreting terrane in the northern Gulf of Alaska. Geology 11:718–721

Caracciolo L, Orlando A, Marchev P, Critelli S, Manetti P, Raycheva R, Riley D (2016) Provenance of Tertiary volcanoclastic sediment in NW Thrace (Bulgaria): evidence from detrital amphibole and pyroxene geochemistry. Sed Geol 336:120–137

Carter A, Riley TR, Hillenbrand CD, Rittner M (2017) Widespread antarctic glaciation during the Late Eocene. Earth Planet Sci Lett 458:49–57

Cawood PA (1983) Modal composition of detrital clinopyroxene geochemistry of lithic sandstones from New England Fold and Belt (east Australia): a Paleozoic terrane forearc. Geol Soc Am Bull 94:199–1214

Cawood PA, Buchan C (2007) Linking accretionary orogenesis with supercontinent assembly. Earth Sci Rev 82:217–256

Childress LB, Ridgway KD (2014) Glacial and tectonic influence on terrestrial organic carbon delivery to high latitude deep marine systems: IODP Site U1417, Surveyor Fan, Gulf of Alaska. AGU Fall Meeting 2014, abstract id. PP23D-05

Childress LB, Ridgway KD, Blair NE, Bahlburg H, Berbel G, Cowan EA, Forwick M, Gulick SP, Jaeger JM, Maerz C, McClymont E, Moy CM, Müller J, Nakamura A, Ribeiro F (2013) Potential links between onshore tectonics and terrestrial organic carbon

delivery to distal submarine fan environments: IODP Site U1417, Surveyor Fan, Gulf of Alaska. AGU Fall Meeting, abstract id. T23D-2624
Clift P, Vannucchi P (2004) Controls on tectonic accretion versus erosion in subduction zones: implications for the origin and recycling of the continental crust. Rev Geophys 42, RG2001. https://doi.org/10.1029/2003RG000127
Clift PD, Giosan L, Henstock TJ, Tabrez AR (2014) Sediment storage and reworking on the shelf and in the Canyon of the Indus River-Fan System since the last glacial maximum. Bas Res 26:183–202
Collins WJ, Belousova EA, Kemp AIS, Murphy JB (2011) Two contrasting Phanerozoic orogenic systems revealed by hafnium isotope data. Nat Geosci 4:333–337
Colpron M, Nelson JL, Murphy DC (2007) Northern Cordilleran terranes and their interactions through time. GSA Today. https://doi.org/10.1130/GSAT01704-5A.1
Coney PJ, Jones DL, Monger JWH (1980) Cordilleran suspect terranes. Nature 288:329–333
Contreras-Reyes E, Flueh E, Grevemeyer I (2010) Tectonic control on sediment accretion and subduction off south central Chile: Implications for coseismic rupture processes of the 1960 and 2010 megathrust earthquakes. Tectonics 29: TC6018.
Coombs DS (1989) Prehnite–pumpellyite facies. In: Petrology. Encyclopedia of Earth Science. Springer, Boston
Dickinson WR (1970) Interpreting detrital modes of greywacke and arkose. J Sed Pet 40:695–707
Dickinson WR (1985) Interpreting provenance relations from detrital modes of sandstones. In: Zuffa GG (ed) Provenance of arenites. NATO ASI Series 148:333–361
Dickinson WR, Suzeck CA (1979) Plate tectonics and sandstone compositions. AAPG Bull 63:2164–2182
Dickinson WR, Beard LS, Brakenridge GR, Erjavec JL, Ferguson RC, Inman KF, Knepp RA, Lindberg FA, Ryberg PT (1983) Provenance of North American Phanerozoic sandstones in relation to tectonic setting. Geol Soc Am Bull 94:222–235
Dott RH (1964) Wacke, graywacke and matrix—what approach to immature sandstone classification. J Sed Pet 34:625–632
Drewer C (2016) Provenanzanalyse an den Proben der Sites U1419 und U1420 der IODP Expedition 341 im Golf von Alaska. MSc Thesis, WWU Münster
Dumoulin JA (1988) Sandstone petrographic evidence and the Chugach-Prince William terrane boundary in southern Alaska. Geology 16:456–460
Dunn CA, Enkelmann E, Ridgway KD, Allen WK (2017) Source to sink evaluation of sediment routing in the Gulf of Alaska and Southeast Alaska: a thermochronometric perspective. J Geophys Res Earth Surf 122:711–734
Elliott JL, Larsen CF, Freymueller JT, Motyka RJ (2010) Tectonic block motion and glacial isostatic adjustment in southeast Alaska and adjacent Canada constrained by GPS measurements. J Geophys Res 115:B09407. https://doi.org/10.1029/2009JB007139
Enami M, Liou JG, Mattinson CG (2004) Epidote minerals in high P/T metamorphic terranes: subduction zone and high- to ultrahigh-pressure metamorphism. Rev Min Geochem 56:347–398
Enkelmann E, Garver JI, Pavlis TL (2008) Rapid exhumation of ice-covered rocks of the Chugach–St. Elias orogen. Southeast Alaska Geol 36:915–918
Enkelmann E, Zeitler PK, Pavlis TL, Garver JI, Ridgway KD (2009) Intense localized rock uplift and erosion in the St Elias orogen of Alaska. Nat Geosci 2:360–363
Enkelmann E, Zeitler PK, Garver JI, Pavlis TL, Hooks BP (2010) The thermochronological record of tectonic and surface process interaction at the Yakutat-North American collision zone in southeast Alaska. Am J Sci 310:231–260
Enkelmann E, Koons PO, Pavlis TL, Hallet B, Barker A, Elliott J, Garver JI, Gulick SPS, Headley RM, Pavlis GL, Ridgway KD, Ruppert N, van Avendonk HJA (2015) Cooperation among tectonic and surface processes in the St. Elias Range, Earth's highest coastal mountains. Geophys Res Let 42:5838–5846
Enkelmann E, Piestrzeniewicz A, Falkowski S, Stübner K, Ehlers TA (2017) Thermochronology in southeast Alaska and southwest Yukon: implications for north american plate response to terrane accretion. Earth Planet Sci Lett 457:348–358
Expedition 341 Scientists (2014) Southern Alaska Margin: interactions of tectonics, climate, and sedimentation. IODP Prel Rep. https://doi.org/10.2204/iodp.pr.341.2014
Falkowski S, Enkelmann E, Ehlers TA (2014) Constraining the area of rapid and deep-seated exhumation at the St. Elias syntaxis, Southeast Alaska, with detrital zircon fission-track analysis. Tectonics 33:597–616
Farris DW, Paterson SR (2009) Subduction of a segmented ridge along a curved continental margin: variations between the western and eastern Sanak-Baranof belt, southern Alaska. Tectonophysics 464:100–117
Finzel ES, Trop JM, Ridgway KD, Enkelmann E (2011) Upper plate proxies for flat-slab subduction processes in southern Alaska. Earth Planet Sci Lett 303:348–360
Finzel ES, Flesch LM, Ridgway KD, Holt WE, Ghosh A (2015) Surface motions and intraplate continental deformation in Alaska driven by mantle flow. Geophys Res Lett 42:4350–4358
Frei D, Liebscher A, Franz G, Dulski P (2004) Trace element geochemistry of epidote minerals. Rev Min Geochem 56:553–605
Garzanti E (2016) From static to dynamic provenance analysis—sedimentary petrology upgraded. Sed Geol 336:3–13
Garzanti E, Andó S (2007) Plate tectonics and heavy mineral suites of modern sands. In: Mange MA, Wright DT (eds) Heavy minerals in use. Develop Sediment 58:741–763
Garzanti E, Doglioni C, Vezzoli G, Andò S (2007) Orogenic belts and orogenic sediment provenance. J Geol 115:315–334
Garzanti E, Andò S, Vezzoli G (2008) Settling-equivalence of detrital minerals and grain-size dependence of sediment composition. Earth Planet Sci Lett 273:138–151
Garzanti E, Andò S, Vezzoli G (2020) Provenance of cenozoic indus fan sediments (IODP Sites U1456 and U1457). J Sed Res 90:1114–1127
Gasser D, Bruand E, Stüwe K, Foster DA, Schuster R, Fügenschuh B, Pavlis T (2011) Formation of a metamorphic complex along an obliquely convergent margin: Structural and thermochronological evolution of the Chugach Metamorphic Complex, southern Alaska. Tectonics 30: TC2012. https://doi.org/10.1029/2010TC002776
Grapes RH, Hoskin PWO (2004) Epidote group minerals in low-medium pressure metamorphic terranes. Rev Min Geochem 56:301–345
Griffiths GA (1979) High sediment yields from major rivers of the Western Southern Alps, New Zealand. Nature 282:61–63
Gulick SPS, Jaeger JM, Mix AC, Asahi H, Bahlburg H, Belanger CL, Berbel GBB, Childress L, Cowan E, Drab L, Forwick M, Fukumura A, Ge S, Gupta S, Kioka A, Konno S, LeVay LJ, März C, Matsuzaki KM, McClymont EL, Moy C, Müller J, Nakamura A, Ojima T, Ribeiro FR, Ridgway KD, Romero OE, Slagle AL, Stoner JS, St-Onge G, Suto I, Walczak MD, Worthington LL, Bailey I, Enkelmann E, Reece R, Swartz JM (2015) Mid-Pleistocene climate transition drives net mass loss from rapidly uplifting St. Elias Mountains. Alaska PNAS 112:15042–15047
Haeussler PJ, Bradley DC, Wells RE, Miller ML (2003) Life and death of the resurrection plate: evidence for its existence and subduction in the northeastern Pacific in Paleocene-Eocene time. Geol Soc Am Bull 115:867–880
Hallet B, Hunter L, Bogen J (1996) Rates of erosion and sediment evacuation by glaciers: a review of field data and their implications. Global Planet Change 12:213–235

Hay WW (1996) Tectonics and climate. Geol Rdsch 85:409–437
Hayes JB (1973) Petrology of indurated sandstones, Leg 18, deep sea drilling project. Proc DSDP Leg 18:915–924
Huber B, Bahlburg H, Berndt J, Dunkl I, Gerdes A (2018a) Provenance of the surveyor fan and precursor sediments in the gulf of alaska—implications of a combined U-Pb, (U-Th)/He, Hf, and rare earth element study of detrital zircons. J Geol 126:577–600
Huber B, Bahlburg H, Pfänder JA (2018b) Single grain heavy mineral provenance of garnet and amphibole in the Surveyor Fan and precursor sediments on the Gulf of Alaska abyssal plain - Implications for climate-tectonic interactions in the St. Elias Orogen Sed Geol 372:173–192
Hudson T, Plafker G (1982) Paleogene metamorphism of an accretionary flysch terrane, eastern Gulf of Alaska. Geol Soc Am Bull 93:1280–1290
Hülscher J, Bahlburg H, Pfänder J (2018) New geochemical results indicate a non-alpine provenance for the Alpine Spectrum (epidote, garnet, hornblende) in Quaternary upper Rhine sediments. Sed Geol 375:134–144
Ingersoll RV, Suczek CA (1979) Petrology and provenance of Neogene sand from the Nicobar and Bengal fans, DSDP Sites 211 and 218. J Sed Pet 49:1217–1228
Ingersoll RV, Bullard TF, Ford RL, Grimm JP, Pickle JD, Sares SW (1984) The effect of grain size on detrital modes: a test of the Gazzi-Dickinson point-counting method. J Sed Res 54:103–116
Jaeger JM, Gulick SPS, LeVay LJ, Asahi H, Bahlburg H, Belanger CL, Berbel GBB, Childress L, Cowan E, Drab L, Forwick M, Fukumura A, Ge S, Gupta S, Kioka A, Konno S, LeVay LJ, März C, Matsuzaki KM, McClymont EL, Moy C, Müller J, Nakamura A, Ojima T, Ribeiro FR, Ridgway KD, Romero OE, Slagle AL, Stoner JS, St-Onge G, Suto I, Walczak MD, Worthington LL (2014) Proc. IODP 341: College Station, TX (Integrated Ocean Drilling Program). https://doi.org/10.2204/iodp.proc.341.103.2014.
Jaeger JM, Salinas JK, Penkrot ML, Bruand M (2017) Persistence of the Pleistocene glacial buzzsaw in the St. Elias Mountains, Alaska. GSA Abstr Prog. https://doi.org/10.1130/abs/2017AM-303894
Jiao R, Herman F, Beyssac O, Adatte T, Cox SC, Nelson FE, Neil HL (2018) Erosion of the Southern Alps of New Zealand during the last deglaciation. Geology 46:975–978
Koons PO, Norris RJ, Craw D, Cooper AF (2003) Influence of exhumation on the structural evolution of transpressional plate boundaries. An example from the Southern Alps. New Zeal Geol 31:3–6
Koppes MN, Montgomery DR (2009) The relative efficacy of fluvial and glacial erosion over modern to orogenic timescales. Nat Geosci 2:644–647
Krawinkel H, Wozazek S, Krawinkel J, Hellmann W (1999) Heavy-mineral analysis and clinopyroxene geochemistry applied to provenance analysis of lithic sandstones from the Azuero-Soná Complex (NW Panama). Sed Geol 24:149–168
Krippner A, Meinhold G, Morton AC, von Eynatten H (2014) Evaluation of garnet discrimination diagrams using geochemical data of garnets derived from various host rocks. Sed Geol 306:36–52
Krynine PD (1937) Petrography and genesis of the Siwalik series. Am J Sci 34:422–446
Kulm LD, von Huene R, et al (1973) Initial reports of the deep sea drilling project, volume 18, Washington (U.S. Government Printing Office), 1–1077
Laberg JS, Vorren TO (2000) Flow behaviour of the submarine glaciogenic debris flows on the Bear Island Trough Mount Fan, western Barents Sea. Sedimentology 47:1105–1117
Lagoe MB, Zellers SD (1996) Climates and climate variability of the pliocene depositional and microfaunal response to Pliocene climate change and tectonics in the eastern Gulf of Alaska. Mar Micropaleontol 27:121–140
Lagoe MB, Eyles CH, Eyles N, Hale C (1993) Timing of late Cenozoic tidewater glaciation in the far North Pacific. Geol Soc Am Bull 105:1542–1560
Lease RO, Haeussler PJ, Witter RC, Stockli DF, Bender AM, Kelsey HM, O'Sullivan PB (2021) Extreme quaternary plate boundary exhumation and strike slip localized along the southern Fairweather fault, Alaska, USA. Geology. https://doi.org/10.1130/G48464.1
Liang W, Garzanti E, Andò S, Gentile P, Resentini A (2019) Multimineral fingerprinting of Transhimalayan and Himalayan sources of Indus-derived Thal Desert sand (Central Pakistan). Minerals 9:457
Lull S, Plafker G (1985) Petrography of sandstone from the Yakutat Group, Malaspina District, Southern Alaska. In: Bartsch-Winkler S, Reed KM (eds) The U.S. Geological Survey in Alaska: Accomplishments during 1983. USGS Surv Circ 945:73–77
Mange MA, Morton AC, 2007. Chapter 13 Geochemistry of Heavy Minerals. In: Mange MA, Wright DT (eds) Developments in sedimentology 58:345–391
Manley WF, Kaufman DS (2002) Alaska paleo-glacier atlas. Institute of Arctic and Alpine Research (INSTAAR), University of Colorado. http://instaar.coloradoq25.edu/QGISL/ak_paleoglacier_atlas
Molnar P, Dahem KE (2010) Major intracontinental strike-slip faults and contrasts in lithospheric strength. Geosphere 6:444–476
Morimoto N, Fabries J, Ferguson AK, Ginzburg IV, Ross M, Seifert FA, Zussman J, Aoki K, Gottardi G (1988) Nomenclature of pyroxenes. Am Mineral 73:1123–1133
Morton AC, Hallsworth CR (2007) Stability of detrital heavy minerals during burial diagenesis. In: Mange MA, Wright DT (eds) Heavy minerals in use. Dev Sediment 58:215–245
Nechaev VP, Isphording WC (1993) Heavy-mineral assemblages of continental margins as indicators of plate-tectonic environments. J Sed Pet 63:1110–1117
Nilsen TH, Zuffa GG (1982) The chugach terrane, a cretaceous trench-fill deposit, southern Alaska. In: Leggett JK (ed) Trench-forearc geology. Geol Soc London Spec Publ 10:213–227
Nisbet EG, Pearce JA (1977) Clinopyroxene composition in mafic lavas from different rectonic settings. Contrib Min Petrol 63:149–160
Pavlis TL, Sisson VB (1995) Structural history of the Chugach metamorphic complex in the Tana River Region, Eastern Alaska: a record of Eocene ridge subduction. Geol Soc Am Bull 107:1333–1355
Pavlis TL, Chapman JB, Bruhn RL, Ridgway K, Worthington LL, Gulick SPS, Spotila J (2012) Structure of the actively deforming fold-thrust belt of the St. Elias orogen with implications for glacial exhumation and three-dimensional tectonic processes. Geosphere 8:991–1019
Penkrot M, Jaeger JM, Loss DP, Bruand E (2017) Persistence of the Pleistocene glacial buzzsaw in the St. Elias Mountains, Alaska. Geol Soc Am Abstr Prog. https://doi.org/10.1130/abs/2017AM-303894
Penkrot ML, Jaeger JM, Cowan EA, Walczak MH, Mix AC, LeVay L (2018) Tectonic and climate influences on spatial and temporal variations of subglacial erosion; Bering Glacier, Alaska. AGU Fall meeting, Abstract id. C51E-1119
Perry S, Garver J, Ridgway K (2009) Transport of the Yakutat Terrane, southern Alaska: evidence from sediment petrology and detrital zircon fission-track and U/Pb double dating. J Geol 117:156–173
Pettijohn FJ, Potter PE, Siever R (1987) Sand and sandstones. 2nd ed. Springer, New York, Berlin, Heidelberg, pp 1–553
Pichler H, Schmitt-Riegraf C (1987) Gesteinsbildende Minerale im Dünnschliff. Enke:1–230
Pickering KT, Carter A, Andò S, Garzanti E, Limonta M, Vezzoli G, Milliken KL (2020a) Deciphering relationships between the

Nicobar and Bengal submarine fans. Indian Ocean Earth Planet Sci Lett 544:116329
Pickering KT, Pouderoux H, McNeill LC, Backman J, Chemale F, Kutterolf S, Milliken KL, Mukoyoshi H, Henstock TJ, Stevens DE, Parnell C, Dugan B (2020b) Sedimentology, stratigraphy and architecture of the Nicobar Fan (Bengal–Nicobar Fan System), Indian Ocean: results from International Ocean Discovery Program Expedition 362. Sedimentology. https://doi.org/10.1111/sed.12701
Plafker G (1987) Regional geology and petroleum potential of the northern Gulf of Alaska continental margin. In: Scholl DW, Grantz A, Vedder JG (eds) Geology and resource potential of the continental margin of western North America and adjacent ocean basins—Beaufort Sea to Baja California. Circum-Pacific Council for Energy and Mineral Resources, Earth Sci. Ser. 6:229–268.
Plafker G, Moore J, Winkler G (1994) Geology of the southern Alaska margin. In: Plafker G, Berg H (eds) The geology of Alaska (Geology of North America, Vol. G-1). Geol Soc Am: 389–449
Post A (1972) Periodic surge origin of folded medial moraines on Bering piedmont glacier. Alaska J Glaciol 11:219–226
Potter PE (1994) Modern sands of South America. Geol Rdsch 83:212–232
Rea DK, Snockx H (1995) Sediment Fluxes in the Gulf of Alaska: paleoceanographic record from Site 887 on the patton-murray seamount platform. In: Rea DK, Basov IA, Scholl DW, Allan JF (eds) Proceedings ODP: scientific results. https://doi.org/10.2973/odp.proc.sr.145.122.1995
Reece RS, Gulick SPS, Horton BK, Christeson GL, Worthington LL (2011) Tectonic and climatic influence on the evolution of the Surveyor fan and channel system, Gulf of Alaska. Geosphere 7:830–844
Reilly BT, Bergmann F, Weber ME, Stoner JS, Selkin P, Meynadier L, Schwenk T, Spiess V, France-Lenord C (2020) Middle to late Pleistocene evolution of the Bengal Fan: integrating core and seismic observations for chronostratigraphic modeling of the IODP Expedition 354 8° north transect. Geochem Geophys Geosyst 21: e2019GC008878
Reimann Zumsprekel C, Bahlburg H, Carlotto V, Boekhout F, Berndt J, Lopez S (2015) Multi-method provenance model for early Paleozoic sedimentary basins of southern Peru and northern Bolivia (13°–18°S). J S Am Earth Sci 64:94–115
Roe GH, Stolar DS, Willett SD (2006) Response of a steady-state critical wedge orogen to changes in climate and tectonic forcing. Geol Soc Am Spec Pap 398:227–239
Rösler HJ (1984) Lehrbuch der mineralogie. VEB Deutscher Verlag für Grundstoffindustrie, Leipzig, pp 1–833
Sample JC, Reid MR (2003) Large-scale, latest Cretaceous uplift along the northeast Pacific Rim: evidence from sediment volume, sandstone petrography, and Nd isotope signatures of the Kodiak Formation, Kodiak Islands, Alaska. In: Sisson VB, Roeske SM, Pavlis TL (eds) Geology of a transpressional orogen developed during ridge-trench interaction along the North Pacific margin. Geol Soc Am Spec Pap 371:51–70
Sisson VB, Hollister LS, Onstott TC (1989) Petrologic and age constraints on the origin of a low-pressure/high-temperature metamorphic complex, southern Alaska. J Geophys Res 94:4392–4410
Sisson VB, Poole AR, Harris NR, Cooper Bruner H, Pavlis TL, Copeland P, Donelick RA, McClelland WC (2003) Geochemical and geochronologic constraints for genesis of a tonalite-trondhjemite suite and associated mafic intrusive rocks in the eastern Chugach Mountains, Alaska: a record of ridge-transform subduction. In: Sisson VB, Roeske SM, Pavlis TL (eds) Geology of a transpressional orogen developed during ridge-trench interaction along the North-Pacific margin. Geol Soc Am Spec Pap 371: 293–326
Spiegel C, Siebel W, Frisch W, Berner Z (2002) Nd and Sr isotopic ratios and trace element geochemistry of epidote from the Swiss Molasse Basin as provenance indicators: implications for the reconstruction of the exhumation history of the Central Alps. Chem Geol 189:231–250
Stevenson AJ, Embley R (1987) Deep-sea fan bodies, terrigenous turbidite sedimentation and petroleum geology, Gulf of Alaska. In: Scholl DW, Grantz A, Vedder JG (eds) Geology and resource potential of the continental margin of western north America and adjacent ocean basins—Beaufort Sea to Baja California. Circum-Pacific Council for Energy and Mineral Resources, AAPG, Houston, 503–522
Thornburg TM, Kulm LD (1987) Sedimentation in the Chile trench: petrofacies and provenance. J Sed Pet 57:55–74
Thornburg TM, Kulm LD, Hussong DM (1990) Submarine-fan development in the southern Chile trench: a dynamic interplay of tectonics and sedimentation. Geol Soc Am Bull 102:1658–1680
Trop JM, Ridgway KD (2007) Mesozoic and cenozoic tectonic growth of southern Alaska: a sedimentary basin perspective. In: Ridgway KD, Trop JM, Glen JMG, O'Neill JM (eds) Tectonic growth of a collisional continental margin: crustal evolution of Southern Alaska. Geol Soc Am Spec Pap 431:55–94
Trop JM, Ridgway KD, Manuszak JD, Layer P (2002) Mesozoic sedimentary-basin development on the allochthonous Wrangellia composite terrane, Wrangell Mountains basin, Alaska: a long-term record of terrane migration and arc construction. Geol Soc Am Bull 114:693–717
Valloni R, Maynard JB (1981) Detrital modes of recent deep-sea sands and their relation to tectonic setting: a first approximation. Sedimentology 28:75–83
Vermeesch P, Resentini A, Garzanti E (2016) An R package for statistical provenance analysis. Sed Geol. https://doi.org/10.1016/j.sedgeo.2016.01.009
von Eynatten H, Dunkl I (2012) Assessing the sediment factory: the role of single grain analysis. Earth Sci Rev 115:97–120
von Eynatten H, Barceló-Vidal C, Pawlowski-Glahn V (2003) Composition and discrimination of sandstones: a statistical evaluation of different analytical methods. J Sed Res 73:47–57
Weltje GJ, von Eynatten H (2004) Quantitative provenance analysis of sediments: review and outlook. Sed Geol 171:1–11
Willett SD, Beaumont C, Fullsack P (1993) Mechanical model for the tectonics of doubly vergent compressional orogens. Geology 21:371–374
Worthington LL, Gulick SPS, Pavlis TL (2010) Coupled stratigraphic and structural evolution of a glaciated orogenic wedge, offshore, St. Elias orogen, Alaska. Tectonics 29: TC6013. https://doi.org/10.1029/2010TC002723
Yanites BJ, Ehlers TA (2012) Global climate and tectonic controls on the denudation of glaciated mountains. EPSL 325–326:63–75
Yavuz F (2013) WinPyrox: a Windows program for pyroxene calculation classification and thermobarometry. Am Mineral 98:1338–1359
Yerino LH, Maynard JB (1984) Petrography of modern sands from the Peru-Chile trench and adjacent areas. Sedimentology 31:83–89
Zuffa GG, Nilsen TH, Winkler GR (1980) Rock-fragment petrography of the upper cretaceous chugach terrane, southern Alaska: USGS Open-File Rep 80–713:1–28